4 Diffusion in Semiconductors

Teh Yu Tan and Ulrich Gösele

4.1 Introduction

This chapter discusses diffusion phenomena in the semiconductors Si, Ge, and GaAs. Silicon and GaAs are the two main materials used in fabricating electronic and optoelectronic devices. Diffusion in Ge will also be mentioned for the reason that it is the simplest case among semiconductors. Diffusion processes are used in doping a semiconductor with n-type and p-type dopant atoms to produce pn-junctions for device operations. The n- and p-type dopants are specific kinds of substitutional impurity species producing the electric carriers electrons (e) and holes (h), respectively, in a semiconductor. Diffusion processes are also involved in the removal of detrimental metallic impurities, in silicide formation and in thermal SiO_2 growth in fabricating devices using Si.

4.2 Diffusion Mechanisms and Point Defects in Semiconductors

Impurity atoms may dissolve in a semiconductor by occupying interstitial (i) or substitutional (s) sites, or both. As in metals (see Chap. 1), atoms of i species in semiconductors migrate directly between the appropriate interstitial sites, which is described well by Fick's second law

$$\frac{\partial C}{\partial t} = D\frac{\partial^2 C}{\partial x^2}\,, \tag{4.1}$$

where D is the diffusivity and C is the concentration. The diffusivity of an i species is characterized by a single activation enthalpy.

The semiconductor crystal host atom self-diffusion and the diffusion of s impurity species utilize native point defects. While the dominant native point defect species in metals are vacancies (V), both V and self-interstitials (I) contribute in semiconductors. To diffuse, an impurity s atom may directly *exchange* or migrate as a *pair or complex* with an I or a V, but only the exchange mechanism is operative for the host crystal atom self-diffusion, which is slower than that of a s species utilizing the same point defect species as diffusion

vehicles via the pairing mechanism. Furthermore, in a semiconductor both V and I can be in several different charge states with their concentrations dependent upon the semiconductor doping level and temperature. These factors lead to complications in the Fick's second law description of self-diffusion and diffusion of substitutional impurities in that the diffusivity shall consist of the contributions of all the involved point defect species which may not be a constant at a given temperature, and may also not reveal a single activation enthalpy over a temperature range. Furthermore, some impurity species are interstitial-substitutional (i-s) species which dissolve predominantly on substitutional sites but their diffusion is actually due to the rapid migration of those occupying interstitial sites and the interchange between atoms occupying the two different types of sites. The diffusivity in the Fick's second law description of the diffusion process of the i-s species is an *effective* diffusivity D^{eff} which may exhibit a strong dependence on its own concentration. These aspects will be examined with the diffusion phenomena of the specific semiconductor.

4.3 Diffusion in Silicon

Because of its use in fabricating integrated circuits, Si is the most important electronic material presently used and is likely to keep that position in the future. Diffusion processes are essential in the electronic device fabrication processes. Figure 4.1 shows the diffusivities of the most important impurities and that of Si self-diffusion. Borrowing the knowledge from metals, diffusion in Si had been first thought to be dominated by V-related mechanisms. In 1968 Seeger and Chik [1] suggested that in Si both V and I contribute to self- and dopant diffusion processes. The problem of the dominant point defect species in Si constituted a controversy for more than 20 years. Finally, during the 1980s [2], it was generally accepted that both I and V have to be taken into account, so as to consistently interpret the results of a large number of different experiments. The main indications for the involvement of I came from experiments performed under non-equilibrium native point defect conditions, such as the influence of surface oxidation or nitridation on dopant diffusion. In this regard, diffusion of the i-s species such as Au or Pt was also crucial. What is still uncertain is the diffusivity and the thermal equilibrium concentration values of I and V, to be mentioned later.

4.3.1 Silicon Self-Diffusion

Because I and V both contribute, the transport of Si self-atoms under thermal equilibrium conditions is governed by the uncorrelated self-diffusion coefficient

$$D_{\text{SD}} = D_I c_I^{\text{eq}} + D_V c_V^{\text{eq}} , \tag{4.2}$$

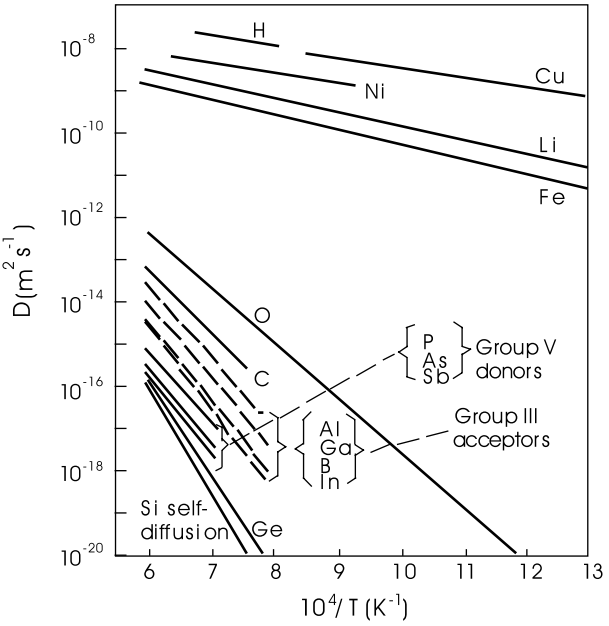

Fig. 4.1. A survey of diffusivity values of the most important impurities in Si and of Si self-diffusion.

where D_I and D_V are respectively the diffusivities of I and V, and $c_I^{\rm eq}$ and $c_V^{\rm eq}$ are respectively the I and V thermal equilibrium concentrations normalized by the appropriate site densities into atomic fractions. As has been mentioned, native point defects may exist in several charge states. The observed doping dependence of group-III and V dopant diffusion (Sect. 4.3.3) indicates the contributions of neutral, positively charged, negatively and doubly negatively charged native point defects, but it is not known whether all these charge states occur for both I and V. Taking all observed charge states into account we may write $D_I c_I^{\rm eq}$ as

$$D_I c_I^{\rm eq} = D_{I^o} c_{I^o}^{\rm eq} + D_{I^+} c_{I^+}^{\rm eq} + D_{I^-} c_{I^-}^{\rm eq} + D_{I^{2-}} c_{I^{2-}}^{\rm eq} \,, \tag{4.3}$$

and an analogous expression for V. The quantity $D_I c_I^{\rm eq}$ comprises the sum of the concentrations of self-interstitials in the various charge states according to

$$c_I^{\rm eq} = c_{I^o}^{\rm eq} + c_{I^+}^{\rm eq} + c_{I^-}^{\rm eq} + c_{I^{2-}}^{\rm eq} \,. \tag{4.4}$$

Therefore, the diffusivity D_I is actually an effective diffusion coefficient consisting of an weighted average of the diffusivities in the different charge states. The same holds analogously for $c_V^{\rm eq}$ and D_V.

Self-diffusion in Si is studied by measuring the diffusion of Si isotope tracer atoms $D_{\rm T}$ which differs slightly from $D_{\rm SD}$ of (4.1), since it contains the correlation factors f_I and f_V in the expression $D_{\rm T} = f_I D_I c_I^{\rm eq} + f_V D_V c_V^{\rm eq}$ (see Chap. 1 for details). In the diamond cubic lattice, $f_V = 0.5$, and $f_I \leq 1$

(depends on the unknown self-interstitial configuration). Measured results for D_{T} are usually fitted to the expression $D_{\mathrm{T}} = D_o \exp(-Q/k_{\mathrm{B}}T)$, where D_o is a pre-exponential factor, Q is the activation enthalpy, k_{B} is Boltzmann's constant and T is absolute temperature. A summary of these results is shown in Fig. 4.2 and elsewhere [3]. Tracer measurements do not allow to separate I and V contributions to self-diffusion. Such a separation became possible by investigating the diffusion of Au, Pt and Zn in Si, described in some detail in Sect. 4.3.2. These experiments allowed a fairly accurate determination of $D_I c_I^{\mathrm{eq}}$ but only a crude estimate of $D_V c_V^{\mathrm{eq}}$ derived from a combination of different types of experiments [2, 3]. The results are

$$D_I c_I^{\mathrm{eq}} = 9.4 \times 10^{-2} \exp(-4.84\,\mathrm{eV}/k_{\mathrm{B}}T)\,\mathrm{m^2 s^{-1}}\,, \tag{4.5}$$

$$D_V c_V^{\mathrm{eq}} = 6 \times 10^{-5} \exp(-4.03\,\mathrm{eV}/k_{\mathrm{B}}T)\,\mathrm{m^2 s^{-1}}\,. \tag{4.6}$$

The values of (4.5) and (4.6) are within the experimental range of the measured Si tracer diffusion coefficient D_{T}. The doping dependence of Si self-diffusion [4] allows to conclude that neutral as well as positively and negatively charged point defects are involved in self-diffusion, but the data are not accurate enough to determine the individual terms of (4.3) or the analogous expression for vacancies. Since D_{T} as well as $D_I c_I^{\mathrm{eq}}$ and $D_V c_V^{\mathrm{eq}}$ each consist of various terms, their representation in terms of an expression of the type of (4.5) and (4.6) can only be an approximation holding over a limited temperature range. In Sect. 4.3.5 we will discuss what is known about the individual factors D_I, c_I^{eq}, D_V and c_V^{eq}.

4.3.2 Interstitial-Substitutional Diffusion: Au, Pt and Zn in Si

Both Au and Pt can reduce minority carrier lifetimes in Si because their energy levels are close to the middle of the band gap. They are used in power devices to improve the device frequency behavior. In contrast, Au and to a lesser extent Pt are undesirable contaminants in integrated circuits and hence have to be avoided or removed. For these reasons, the behavior of Au and Pt has been investigated extensively. Zinc is not a technologically important impurity in Si, but scientifically it served as an example with diffusion behavior in between substitutional dopants and Au and Pt in Si.

These impurities are i-s species dissolved mainly on substitutional sites ($\mathrm{A_s}$) but accomplish diffusion by switching over to an interstitial configuration ($\mathrm{A_i}$) in which their diffusivity $\mathrm{D_i}$ is extremely high. The change-over from i-site to s-site and vice versa involves native point defects. For uncharged species the two basic forms of the i-s change-over processes are the kick-out (KO) mechanism involving I [4, 5]

$$\mathrm{A_i} \Leftrightarrow \mathrm{A_s} + I\,, \tag{4.7}$$

and the much earlier proposed dissociative mechanism or Frank-Turnbull (FT) mechanism involving V [6]

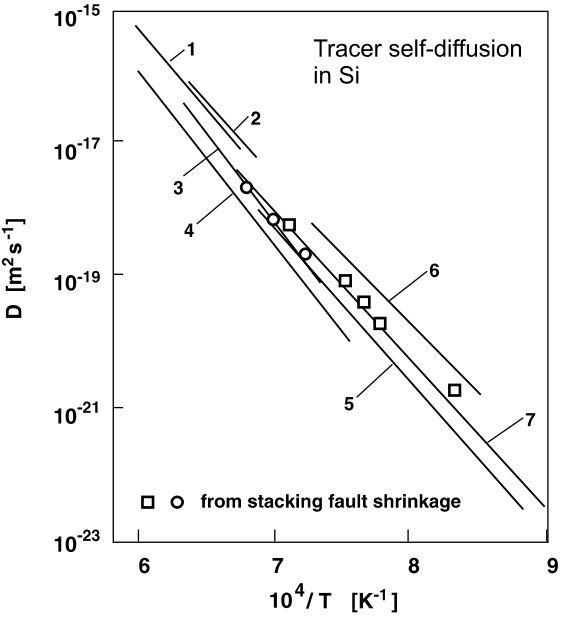

Fig. 4.2. Tracer self-diffusion coefficients of silicon as a function of reciprocal temperature. Partly from [4].

1. R.F. Peart: Phys. Stat. Sol. **15**, K119 (1966)
2. R.N. Ghostagore: Phys. Rev. Lett. **16**, 890 (1966)
3. J.M. Fairfield, B.J. Masters: J. Appl. Phys. **38**, 3148 (1967)
4. J.J. Mayer, H. Mehrer, K. Maier: Inst. Phys. Conf. Ser. **31**, 186K (1977)
5. L. Kalinowski, R. Seguin: Appl. Phys. Lett. **35**, 171 (1980)
6. J. Hirvonen, A. Antilla: Appl. Phys. Lett. **35**, 703 (1979)
7. F.J. Demond, S. Kalbitzer, H. Mannsperger, H. Damjantschitsch: Phys. Lett. **93A**, 503 (1983)

$$A_i + V \Leftrightarrow A_s \,. \tag{4.8}$$

Both mechanisms are schematically shown in Fig. 4.3. The KO mechanism is closely related to the interstitialcy mechanism. The main difference is that the foreign atom, once in an interstitial position, remains there for only one step in the interstitialcy mechanism and for many steps in the KO mechanism. In contrast, the FT mechanism and the vacancy exchange mechanism are qualitatively different. For the vacancy exchange mechanism an increase in V concentration enhances the diffusivity, whereas for the FT mechanism an increase in V concentration rather decreases the diffusivity of the substitutional species.

For a detailed description of i-s atoms diffusing via the KO or FT mechanism, it requires to solve a coupled system of three partial differential equations describing diffusion and reaction of A_i, A_s and the native point defect

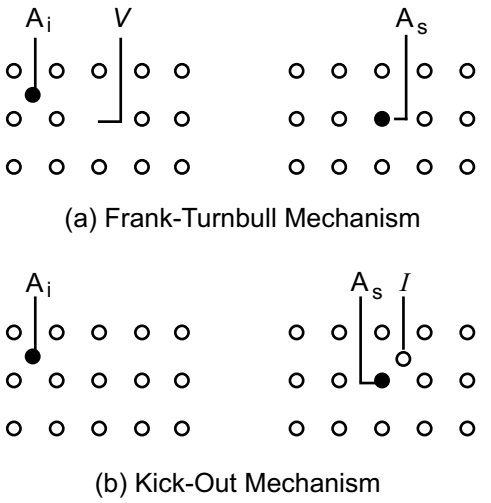

Fig. 4.3. Schematic representation of the Frank-Turnbull mechanism (a) and the kick-out mechanism (b).

involved, V or I [4]. But for cases of in-diffusion from the surface the profile shapes are described well by an *effective* diffusivity D^{eff} obtained for use in the Fick's second law representation, (4.1), of the A_s diffusion process. This requires to assume that the local equilibrium conditions in accordance with reactions (4.7) and (4.8) are

$$C_s C_I / C_i = C_s^{eq} C_I^{eq} / C_i^{eq} , \tag{4.9}$$

$$C_i C_V / C_s = C_i^{eq} C_V^{eq} / C_s^{eq} , \tag{4.10}$$

where C_s and C_i are respectively the concentrations of the s and i atoms of the i-s species, holds for the KO and FT mechanisms, respectively. For the KO mechanism, if the in-diffusion of A_i is slow enough to allow the Is generated to migrate out to the surface to keep their thermal equilibrium concentration (i.e., $D_i C_i^{eq} \ll D_I C_I^{eq}$ holds), then the effective diffusivity of A_s is given by

$$D_{(i)}^{\text{eff}} = D_i C_i / C_s^{eq} , \tag{4.11}$$

provided $C_s^{eq} \gg C_i^{eq}$ holds, which is generally the case. Here the lower index in bracket indicates the rate limiting species. If on the other hand the in-diffusion of A_i is so fast that the generated I cannot escape quickly enough to the surface (i.e., $D_i C_i^{eq} \gg D_I C_I^{eq}$ holds) a supersaturation of I will develop and further incorporation of A_s is limited by the out-diffusion of the generated Is to the surface. This leads to an effective A_s diffusivity $D_{(I)}^{\text{eff}}$ given by

$$D_{(I)}^{\text{eff}} = \left(D_I D_I^{eq} / C_s^{eq}\right) \left(C_s^{eq} / C_s\right)^2 . \tag{4.12}$$

For the FT mechanism, sufficiently slow in-diffusion $D_i C_i^{eq} \ll D_V C_V^{eq}$ leads to the same $D_{(i)}^{\text{eff}}$ as given by (4.11). An effective A_s diffusivity $D_{(V)}^{\text{eff}}$ controlled

by the in-diffusion of V from the surface results, if $D_{\mathrm{i}}C_{\mathrm{i}}^{\mathrm{eq}} \gg D_V C_V^{\mathrm{eq}}$ holds, which reads

$$D_{(V)}^{\mathrm{eff}} = D_V C_V^{\mathrm{eq}} / C_{\mathrm{s}}^{\mathrm{eq}} \,. \tag{4.13}$$

The strongly concentration-dependent effective diffusivity $D_{(i)}^{\mathrm{eff}}$ of (4.12) leads to an A_s concentration profile so strongly deviated away from the erfc-type that it is actually concave upward in $\log C_{\mathrm{s}}$ plotted as a function of $1/\mathrm{T}$. These profiles can easily be distinguished from the erfc-type profiles which are associated with $D_{(V)}^{\mathrm{eff}}$. This macroscopic difference allows one not only to decide between different atomistic diffusion mechanisms of the specific foreign atom involved but also to obtain information on the mechanism of self-diffusion. The effective diffusivities given by (4.12) and (4.13) have been derived under the assumption of dislocation-free crystals. The presence of a high density of dislocations in an elemental crystal maintains the equilibrium concentration of intrinsic point defects and thus an erfc-type profile characterized by the constant diffusivity $D_{(\mathrm{i})}^{\mathrm{eff}}$ of (4.11) will result even if $D_{\mathrm{i}}C_{\mathrm{i}}^{\mathrm{eff}} \gg D_I C_I^{\mathrm{eq}}$ holds. For compound semiconductors this statement does not hold in general, since the presence of dislocations does not necessarily guarantee native point defects to attain their thermal equilibrium concentrations. If I and V co-exist, such as in the case of Si, the effective A_s diffusion coefficient in dislocation-free material for $D_{\mathrm{i}}C_{\mathrm{i}}^{\mathrm{eq}} \gg (D_I C_I^{\mathrm{eq}} + D_V C_V^{\mathrm{eq}})$ is given by

$$D_{(I,V)}^{\mathrm{eff}} = D_{(I)}^{\mathrm{eff}} + D_{(V)}^{\mathrm{eff}} \,. \tag{4.14}$$

The in-diffusion profiles of both Au and Pt in dislocation-free Si show the concave profile shape typical for the KO mechanism [4, 7, 8]. Examples are shown in Figs. 4.4 and 4.5 respectively for Au and for Pt. From profiles like these and from the measured solubility $C_{\mathrm{s}}^{\mathrm{eq}}$ of $\mathrm{Au_s}$ and $\mathrm{Pt_s}$ in Si, the values of $D_I c_I^{\mathrm{eq}}$ given by (4.5) have been determined. Diffusion of Au into thin Si wafers leads to characteristic U-shaped profiles even if the Au has been deposited on one side only. The increase of the Au concentration in the center of the wafer has also been used to determine $D_I c_I^{\mathrm{eq}}$ [6].

In heavily dislocated Si the dislocations act as efficient sinks for I to keep C_I close to C_I^{eq} so that the constant effective diffusivity $D_{(\mathrm{i})}^{\mathrm{eff}}$ of (4.11) governs the A_s profile, which is erfc-shaped. This has been observed by Stolwijk et al. for Au [9]. Analysis of the resulting erfc-profiles yielded

$$D_{\mathrm{i}} c_{\mathrm{i}}^{\mathrm{eq}} \approx 6.4 \times 10^{-3} \exp\left(-3.93\,\mathrm{eV}/k_{\mathrm{B}}T\right)\ \mathrm{m^2 s^{-1}} \,. \tag{4.15}$$

This $D_{\mathrm{i}} c_{\mathrm{i}}^{\mathrm{eq}}$ value turns out to be much larger than $D_I c_I^{\mathrm{eq}}$ given by (4.5), which is consistent with the observation that $\mathrm{Au_s}$ concentration profiles are governed by $D_{(I)}^{\mathrm{eff}}$ in dislocation-free Si.

Zinc diffusion in Si has also been investigated [10]. In highly dislocated material, an erfc-profile develops as expected. In dislocation-free material only the profile part close to the surface shows the concave shape typical for the kickout diffusion mechanism. For lower Zn concentrations, a constant

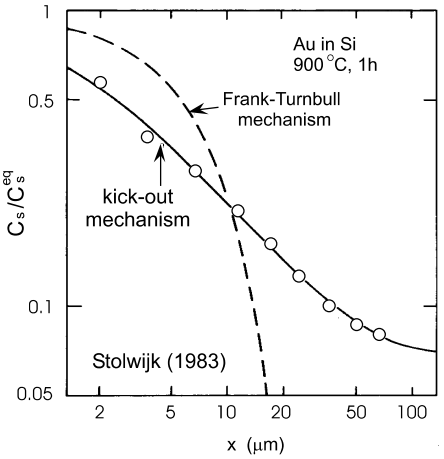

Fig. 4.4. Experimental Au concentration profile in dislocation-free Si (circles) compared with predictions of the Frank-Turnbull and the kick-out mechanism. From [7].

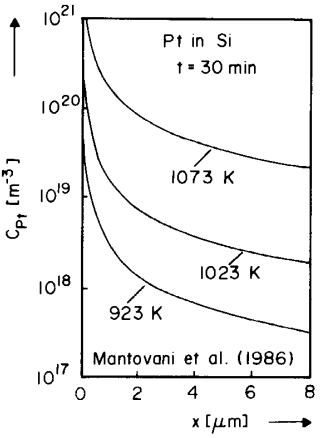

Fig. 4.5. Platinum concentration profiles in dislocation-free Si. From [8].

diffusivity takes over. The reason for this change-over from one profile type to another is as follows. In contrast to the case of Au, the $D_i c_i^{eq}$ value determined for Zn is not much higher than $D_I c_I^{eq}$ so that even in dislocation-free Si only the profile close to the surface is governed by $D_{(I)}^{eff}$ of (4.12) which strongly increases with depth. For sufficiently large penetration depths $D_{(I)}^{eff}$ finally exceeds $D_{(i)}^{eff}$ and a constant effective diffusivity begins to determine the concentration profile. A detailed analysis of this situation can be found elsewhere [3]. The change-over from a concave to an erfc-type profile has also been observed for the diffusion of Au either into very thick Si samples [11] or for short-time diffusion [12] into normal silicon wafers 300–800 μm in thickness.

4.3.3 Dopant Diffusion

Fermi Level Effect

Dopant diffusion has been studied extensively because of its importance in device fabrication. A detailed quantitative understanding of dopant diffusion is also a pre-requisite for accurate and meaningful modeling in numerical process simulation programs. It is not our intention to compile all available data on dopant diffusion in silicon, which may conveniently be found elsewhere (see [3] for a list of references). We will instead concentrate on the diffusion mechanisms and native point defects involved in dopant diffusion,

the effect of the Fermi level on dopant diffusion and on non-equilibrium point defect phenomena induced by high-concentration in-diffusion of dopants.

The diffusivities D_s of all dopants in Si depend on the Fermi level. The experimentally observed doping dependencies may be described in terms of the expression

$$D_\mathrm{s}(n) = D_\mathrm{s}^0 + D_\mathrm{s}^+(n_\mathrm{i}/n) + D_\mathrm{s}^-(n/n_\mathrm{i}) + D_\mathrm{s}^{2-}(n/n_\mathrm{i})^2\,, \tag{4.16}$$

which reduces to

$$D_\mathrm{s}(n_\mathrm{i}) = D_\mathrm{s}^0 + D_\mathrm{s}^+ + D_\mathrm{s}^- + D_\mathrm{s}^{-2} \tag{4.17}$$

for intrinsic conditions $n = n_\mathrm{i}$. Depending on the specific dopant, some of the quantities in (4.17) may be negligibly small. $D_\mathrm{s}(n_\mathrm{i})$ is an exponential function of inverse temperature as shown in Fig. 4.1. Values of these quantities in terms of pre-exponential factors and activation enthalpies are given in Table 4.1. Conflicting results exist on the doping dependence of Sb.

Table 4.1. Diffusion data of various dopants fitted to (4.17). Each term fitted to $D_0 \exp(-Q/k_\mathrm{B}T)$; D_0 values in $10^{-4}\,\mathrm{m^2 s^{-1}}$ and Q values in eV

element	D_0^0	Q^0	D_0^+	Q^+	D_0^-	Q^-	D_0^{2-}	Q^{2-}
B	0.037	3.46	0.72	3.46	–	–	–	–
P	3.85	3.66	–	–	4.44	4.00	44.20	4.37
As	0.066	3.44	–	–	12.0	4.05	–	–
Sb	0.214	3.65	–	–	15.0	4.08	–	–

The higher diffusivities of all dopants as compared to self-diffusion requires faster moving complexes formed by the dopants and native point defects. The doping dependence of $D_\mathrm{s}(n)$ is generally explained in terms of the various charge states of the native point defects carrying dopant diffusion. Since both I and V can be involved in dopant diffusion each of the terms in (4.17) in general consists of an I and a V related contribution, e.g.,

$$D_\mathrm{s}^+ = D_\mathrm{s}^{I^+} + D_\mathrm{s}^{V^+}\,. \tag{4.18}$$

$D_\mathrm{s}(n)$ may also be written in terms of I- and V-related contributions as

$$D_\mathrm{s}(n) = D_\mathrm{s}^I(n) + D_\mathrm{s}^V(n) \tag{4.19}$$

with

$$D_\mathrm{s}^I(n) = D_\mathrm{s}^{I^o} + D_\mathrm{s}^{I^+}(n_\mathrm{i}/n) + D_\mathrm{s}^{I^-}(n/n_\mathrm{i}) + D_\mathrm{s}^{I^{2-}}(n/n_\mathrm{i})^2 \tag{4.20}$$

and an analogous expression for $D_\mathrm{s}^V(n)$.

Contrary to a common opinion, the observed doping dependence expressed in (4.16) just shows that charged point defects are involved in the

diffusion process, but nothing can be learned on the relative contributions of I and V in the various charge states. Strictly speaking, in contrast to the case of self-diffusion, the doping dependence of dopant diffusion does not necessarily prove the presence of charged native point defects but rather the presence of charged point-defect/dopant complexes. In Sect. 4.3.3 we will describe a way to determine the relative contribution of I and V to dopant diffusion by measuring the effect of non-equilibrium concentrations of native point defects on dopant diffusion.

Influence of Surface Reactions

Thermal oxidation is a standard process for forming field and gate oxides, or oxides protecting certain device regions from ion implantation in Si device fabrications. The oxidation process leads to the injection of I which can enhance the diffusivity of dopants using mainly I as diffusion vehicles or retard diffusion of dopants which diffuse mainly via a V mechanism. Oxidation-enhanced diffusion (OED) has been observed for the dopants B, Al, Ga, P and As, and oxidation-retarded diffusion (ORD) was observed for Sb [2–4]. OED is explained by the I supersaturation and that the dopants diffuse via mainly the interstitialcy mechanism. On the other hand, ORD of Sb is explained in terms of the I-V recombination reaction $I + V \Leftrightarrow \phi$, where ϕ is a lattice atom, which leads to

$$C_I C_V = C_I^{\mathrm{eq}} C_V^{\mathrm{eq}}\,, \tag{4.21}$$

and that Sb diffuses mainly via the vacancy mechanism. The presence of an I supersaturation leads to a V undersaturation as described by (4.21). The oxidation-induced I may also nucleate and form I-type dislocation loops on (111) planes containing a stacking fault and are therefore termed oxidation-induced stacking faults (OSF).

The physical reason for the I injection during surface oxidation is as follows [2]. Oxidation occurs by the diffusion of oxygen through the oxide layer to react with the Si crystal atoms at the SiO_2/Si interface. The oxidation reaction is associated with a volume expansion of about a factor of two which is mostly accommodated by viscoelastic flow of the oxide but partly also by the injection of Si interstitials into the Si crystal matrix which leads to an I supersaturation. Oxidation can also cause V injection provided the oxidation occurs at sufficiently high temperatures (typically 1150°C or higher) and the oxide is thick enough. Under these circumstances, Si, probably in the form of SiO [13, 14], diffuses from the interface and reacts with oxygen in the oxide away from the interface. The resulting supersaturation of V associated with an undersaturation of I gives rise to ORD of B and P diffusion [15] and OED of Sb [16]. Thermal nitridation of Si surfaces also causes a supersaturation of V coupled with an undersaturation of I, whereas oxynitridation (nitridation of oxides) behaves more like normal oxidation. Silicidation reactions have

also been found to inject native point defects and to cause enhanced dopant diffusion [17, 18].

A simple quantitative formulation of oxidation- and nitridation-influenced diffusion is based on (4.19), which changes with perturbed native point-defect concentrations C_I and C_V approximately to

$$D_{\mathrm{s}}^{\mathrm{per}}(n) = D_{\mathrm{s}}^{I}(n)\,[C_I/C_I^{\mathrm{eq}}(n)] + D_{\mathrm{s}}^{V}(n)\,[C_V/C_V^{\mathrm{eq}}(n)]\ . \tag{4.22}$$

For long enough times and sufficiently high temperatures (e.g., one hour at 1100°C) local dynamical equilibrium between V and I according to (4.21) is established and (4.22) may be reformulated in terms of C_I/C_I^{eq}. Defining the normalized diffusivity enhancement as $\Delta_{\mathrm{s}}^{\mathrm{per}} = [D_{\mathrm{s}}^{\mathrm{per}}(n) - D_{\mathrm{s}}(n)]/D_{\mathrm{s}}(n)$, the fractional interstitialcy diffusion component as $\Phi_I(n) = D_{\mathrm{s}}^{i}(n)/D_{\mathrm{s}}(n)$, and the I supersaturation ratio as $s_I(n) = [C_I - C_I^{\mathrm{eq}}(n)]/C_I^{\mathrm{eq}}(n)$, (4.22) may be rewritten as [2, 13]

$$\Delta_{\mathrm{s}}^{\mathrm{per}}(n) = \left[2\Phi_I(n) + S_I\Phi_I(n) - 1\right]/(1 + s_I) \tag{4.23}$$

with (4.21) holding. Usually (4.23) is given for intrinsic conditions and the dependence of Φ_I on n is not indicated. Equation (4.23) is plotted in Fig. 4.6 for Φ_I values of 0.85, 0.5 and 0.2.

The left-hand side of Fig. 4.6, where $s_I < 0$ (associated with a V supersaturation) has been realized by high-temperature oxidation and thermal nitridation of silicon surfaces, as mentioned above. Another possibility to generate a vacancy supersaturation is the oxidation in an HCl containing atmosphere at sufficiently high temperatures and for sufficiently large HCl contents [2]. As expected, $s_I < 0$ results in enhanced Sb diffusion and retarded diffusion of P and B. Arsenic diffusion is enhanced as in the case of oxidation, which indicates that arsenic has appreciable components via both V and I ($\Phi_I \sim 0.5$).

Several different procedures have been used to evaluate Φ_I for the different dopants, resulting in a wide range of conflicting published Φ_I values. With the availability of oxidation for generating a self-interstitial supersaturation ($s_I > 0$) and of thermal nitridation for generating a vacancy supersaturation ($s_I < 0$), the most accurate procedure to determine Φ_I appears to be the following: check for the diffusion changes under oxidation and under nitridation conditions. If for $s_I > 0$ the diffusion is enhanced and for $s_I < 0$ it is retarded (as for P and B) then $\Phi_I > 0.5$ holds. Based on the largest observed retardation $\Delta_{\mathrm{s}}^{\mathrm{per}}(\mathrm{min})$, which has a negative value, a lower limit of Φ_I may be estimated according to

$$\Phi_I > 0.5 + 0.5\left[1 - \left(1 + \Delta_{\mathrm{s}}^{\mathrm{per}}(\mathrm{min})^2\right)\right]^{1/2} \tag{4.24}$$

Analogously, an upper limit for Φ_I may be estimated for the case when retarded diffusion occurs for $s_I > 0$ and enhanced diffusion for $s_I < 0$, as in the case of Sb. A different procedure is required for elements with Φ_I values close to 0.5, such as As.

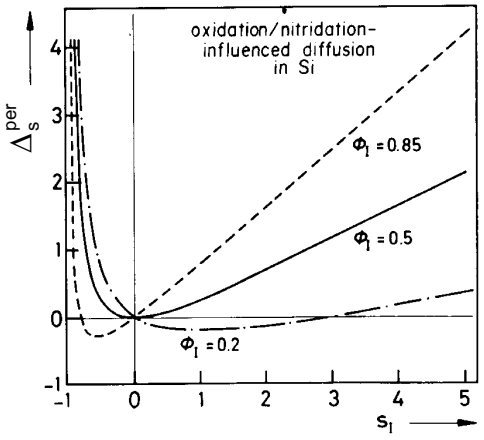

Fig. 4.6. Normalized diffusion enhancement Δ_s^{per} versus self-interstitial supersaturation $s_I = (C_I - C_I^{eq})/C_I^{eq}$ for different values of Φ_I. From [2, 13].

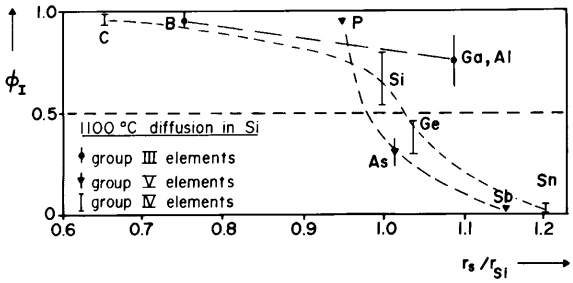

Fig. 4.7. Interstitial-related fractional diffusion component ϕ_I for group III, IV and V elements versus their atomic radius in units of the atomic radius r_{Si} of silicon. The values for carbon and tin are expected from theoretical considerations and limited experimental results. From [3].

In Fig. 4.7 values of Φ_I at 1100°C are shown as a function of the atomic radius r_s of the various dopants for intrinsic doping conditions. Both the charge state (group III or V dopants) and the atomic size influence Φ_I. Φ_I has a tendency to increase with increasing temperature. Oxidation and nitridation experiments and extrinsic conditions indicate a decreasing value of Φ_I for P with increasing n-doping, but both P and B still remain dominated by I ($\Phi_I(n) > 0.5$).

Dopant-Diffusion-Induced Non-Equilibrium Effects

Non-equilibrium concentrations of native point defects may be induced not only by various surface reactions, but also by the in-diffusion of some dopants starting from a high surface concentration. These non-equilibrium effects are most pronounced for high-concentration P diffusion, but also present for other dopants such as B and to a lesser extend for Al and Ga. Phosphorus in-diffusion profiles (Fig. 4.8) show a tail in which the P diffusivity is much

higher (up to a factor of 100 at 900°C) than expected from isoconcentration studies. In n-p-n transistor structures in which high-concentration P is used for the emitter diffusion, the diffusion of the base dopant B below the P diffused region is similarly enhanced, the so-called 'emitter-push effect'. The diffusion of B, P, or Ga in buried layers many microns away from the P diffused region is also greatly enhanced. In contrast, the diffusion of Sb in buried layers is retarded under the same conditions. The enhanced and retarded diffusion phenomena are analogous to those occurring during surface oxidation. As has also been confirmed by dislocation-climb experiments [19], all these phenomena are due to a supersaturation of I, associated with an undersaturation of V, induced by high-concentration in-diffusion of P. The basic features of high-concentration P diffusion are schematically shown in Fig. 4.9, which also indicates the presence of electrically neutral precipitates at P concentrations exceeding the solubility limit at the diffusion temperature. A much less pronounced supersaturation of I is generated by B starting from a high surface concentration as can be concluded from the B profiles and from the growth of interstitial-type stacking faults induced by B diffusion [20, 21].

Many models have been proposed to explain the phenomena associated with high-concentration P diffusion. The earlier models are vacancy based and predict a P-induced V supersaturation which contradict the experimental results obtained in the meantime. In 1986, Morehead and Lever [21] presented a mathematical treatment of high-concentration dopant diffusion which is primarily based on the point-defect species dominating the diffusion of the dopant, e.g., I for P and B and V for Sb. The concentration of the other native point-defect type is assumed to be determined by the dominating point defect via the local equilibrium condition, (4.21). The dopant-induced self-interstitial supersaturation s_I may be estimated by the influx of dopants which release part of the I involved in their diffusion process. These self-interstitials will diffuse to the surface where it is assumed that $C_I = C_I^{\mathrm{eq}}$ holds, and also into the Si bulk. Finally, a quasi-steady-state supersaturation of self-interstitials will develop for which the dopant-induced flux of injected I just cancels the flux of I to the surface. Figure 4.9 shows schematically the situation.

4.3.4 Diffusion of Carbon and Other Group IV Elements

The group IV elements carbon C, Ge and Sn dissolve in Si substitutionally, but knowledge on their diffusion mechanisms is incomplete. Ge and Sn diffusion are similarly slow as Si self-diffusion, whereas C diffusion is much faster (Fig. 4.1).

Germanium atoms are slightly larger than Si atoms. Oxidation and nitridation experiments show a Φ_I value of Ge around 0.4 at 1100°C [24] which is slightly lower than that derived for Si self-diffusion. Diffusion of the much larger Sn atoms in Si is expected to be almost entirely due to the vacancy

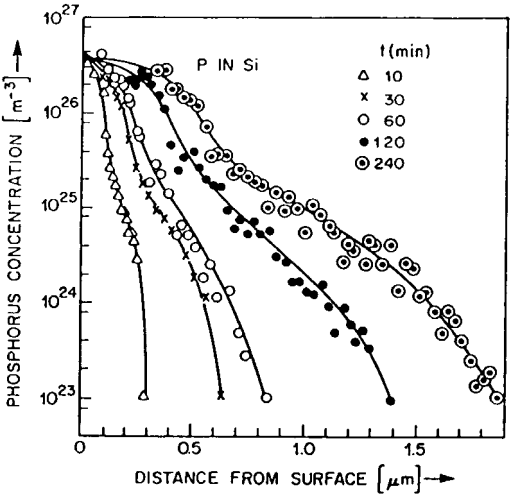

Fig. 4.8. Concentration profiles of P diffused into Si at 900°C for the times t indicated. From [22].

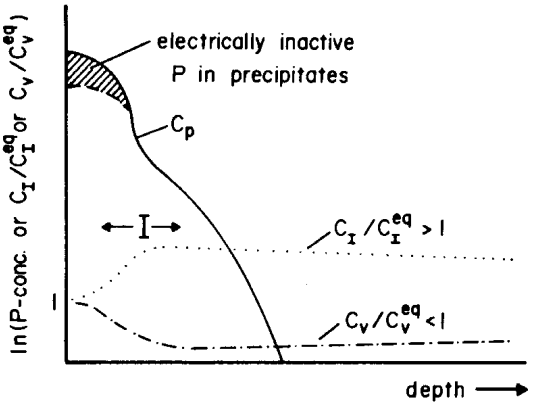

Fig. 4.9. A schematic P concentration profile (C_P) and the normalized native point-defect concentrations C_I/C_I^{eq} and C_V/C_V^{eq}. From [23].

exchange mechanism, similar as for the group V dopant Sb. Consistent with this expectation, a nitridation-induced supersaturation of V increases Sn diffusion [25]), but no quantitative determination of Φ_I is available for Sn.

In-diffusion C profiles in Si are error function-shaped. Considering the atomic volume, it can be expected that the diffusion of C atoms, which are much smaller than Si, involves mainly Si interstitials. Based on EPR measurements, Watkins and Brower [26] proposed 29 years ago that C diffusion is accomplished by a highly mobile CI complex according to $C_s + I \Leftrightarrow CI$, where C_s denotes substitutional C. This is consistent with the experimental observation that I injected by oxidation or high-concentration P in-diffusion enhance C diffusion [27]. Equivalently, we may regard C as an i-s impurity, just as Au. That is, to regard the diffusion of C according to [28, 29]

$$C_s + I \Leftrightarrow C_i \tag{4.25}$$

where C_i denotes an interstitial carbon atom. Since whether C_s diffusion is actually carried by CI complexes or by C_i atoms have not yet been distinguished on a physical basis, and the mathematical descriptions for both cases are identical in form, we can regard C_s diffusion as being carried by C_i atoms in accordance with the KO mechanism of the i-s impurities. Under this assumption, diffusion of C into Si for which the substitutional C concentration is at or below the solubility of the substitutional carbon atoms, C_s^{eq}, the substitutional C diffusivity D_s^{eff} is given by the effective diffusivity $D_i C_i^{eq}/C_s^{eq}$ where D_i is the diffusivity of the fast diffusing C_i atoms and C_i^{eq} is the solubilities of the C_i atoms. Error function type C_s in-diffusion profiles obtain under in-diffusion conditions, because

$$D_s^{eff} C_s^{eq} = D_i C_i^{eq} < D_I C_I^{eq} \tag{4.26}$$

holds. Under this condition, C in-diffusion induced Si interstitials migrated rapidly out to the Si surface and hence the C_I^{eq} condition is basically maintained, in agreement with experimental observations [30,31].

From the C in-diffusion data, the solubility of C_s is given by [30,31]

$$C_s^{eq} = 4 \times 10^{30} \exp(-2.3\,\mathrm{eV}/k_B T)\,\mathrm{m}^{-3} \tag{4.27}$$

and the diffusion coefficient of C_s is given by

$$D_s = 1.9 \times 10^{-4} \exp(-3.1\,\mathrm{eV}/k_B T)\,\mathrm{m}^2\mathrm{s}^{-1}\,. \tag{4.28}$$

Interpreted in accordance with the i-s nature of C, we obtain

$$C_i^{eq} = 2 \times 10^{31} \exp(-4.52\,\mathrm{eV}/k_B T)\,\mathrm{m}^{-3}\,, \tag{4.29}$$

$$D_i = 4.4 \times 10^{4} \exp(-0.88\,\mathrm{eV}/k_B T)\,\mathrm{m}^2\mathrm{s}^{-1}\,. \tag{4.30}$$

For out-diffusion of C_s pre-introduced to high concentrations, however, the situation is very different. For cases for which the C_s concentration significantly exceeded its solubility, as pointed out by Scholz et al. [32],

$$D_i C_i^{eq} > D_I C_I^{eq} \tag{4.31}$$

may be satisfied, leading to a severe undersaturation of I in the high C_s concentration region which significantly retard the out-diffusion of C_s atoms from the region. Indeed, such phenomena have been observed by Rücker et al. [33] and by Werner et al. [34]. These experiments were performed using molecular beam epitaxy (MBE) grown Si layers containing regions with C_s concentrations in the 10^{25} to $10^{26}\,\mathrm{m}^{-3}$ range, and hence tremendously exceeded the C_s solubility of the experimental temperature. A similar retardation of the diffusion of other impurity species diffusing via primarily I, e.g., B, in the same region is also expected. This is indeed the case of the experimental results of Rücker et al. [33], see Fig. 4.10. In order to highly satisfactorily fit both the C_s profile as well as all the B spike-region profiles, Scholz et al. [32]

found that additionally the contribution of Si V must also be included. Vacancy contributes a component to C_s diffusion via the dissociative or FT mechanism as given by reaction (4.8) and a component to B diffusion via the vacancy-pairing mechanism. The V contribution to C_s diffusion is important in regions outside the initial C_s high-concentration region and to B diffusion in all regions.

Using similarly grown samples containing C_s and B spikes, ion implantation induced Si interstitials were found to be substantially attenuated in the C_s spike regions so that the diffusion of B buried beneath the C_s spikes were severely retarded when compared to cases of having no C_s spikes [35]. The phenomenon was interpreted by the authors as due to the reaction $C_s + I \Leftrightarrow CI$ but with the so formed CI complexes assumed to be *immobile*, which is in contrast to the suggestion of Watkins and Brower [26]. The assumption that immobile CI complexes are responsible for the retarded boron diffusion is not needed in the analysis of Scholz et al. [32]. It is expected that ion implantation or oxidation induced Si I supersaturation will enhance the diffusion of C and B with C in concentrations to a moderate level, e.g., in the range of $10^{23}\,\mathrm{m}^{-3}$.

4.3.5 Diffusion of Si Self-Interstitials and Vacancies

For Si, although the product $D_I C_I^{\mathrm{eq}}$ is known and estimates of $D_V C_V^{\mathrm{eq}}$ are available, our knowledge of the individual factors D_I, D_V, C_I^{eq} and C_V^{eq} is limited in spite of immense experimental efforts to determine these quantities. These individual quantities enter most numerical programs for simulating device processing and their elusiveness hinders progress in this area [36].

The most direct way of measuring D_I is the injection of I (e.g., via surface oxidation) at one location of the Si crystal and the observation of its effect on dopant diffusion or on growth or shrinkage of stacking faults at another location as a function of time and of distance between the two locations. That is, the two locations may be the front- and the backside of a Si wafer. Extensive experiments on the spread of oxidation-induced I through wafers by Mizuo and Higuchi [37] have shown that a supersaturation of I arrives at about the same time as a corresponding undersaturation of V. Therefore, these kind of experiments at 1100°C just give information on an effective diffusivity of a perturbation in the I and V concentrations. This effective diffusivity may be expressed approximately by [2]

$$D_{(I,V)}^{\mathrm{eff}} \approx \left(D_I C_I^{\mathrm{eq}} + D_V C_V^{\mathrm{eq}}\right) / \left(C_I^{\mathrm{eq}} + C_V^{\mathrm{eq}}\right) \tag{4.32}$$

and probably corresponds to the diffusivity values of about $3 \times 10^{-13}\,\mathrm{m}^2\,\mathrm{s}^{-1}$ in the experiments of Mizuo and Higuchi at 1100°C [37]. Much efforts had been expended on this approach in the past but the results are inconsistent.

In most experiments aimed at determining D_I it has not been taken into account that I may react with V according to the reaction $I + V \Leftrightarrow \phi$ which

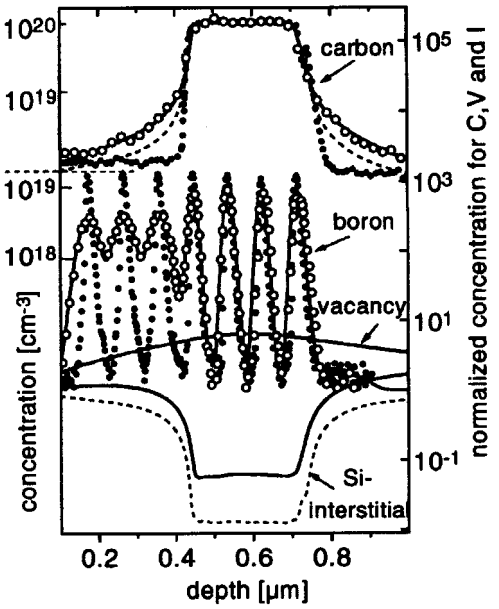

Fig. 4.10. SIMS profiles of a 300 nm thick carbon layer with seven boron spikes [33]. Filled and open circles are respectively data of as-grown and annealed (900°C/45 min) cases. Dashed fitting lines are those with only the kick-out model, and solid lines are those with the dissociative mechanism also included. From [32].

establishes local dynamical equilibrium condition given by (4.21). Based on experiments on oxidation-retarded diffusion of antimony [18, 38] it has been estimated that an astonishingly long time, about one hour, is required to establish local dynamical equilibrium at 1100°C. This long recombination time indicates the presence of an energy or entropy barrier slowing down the recombination reaction. At lower temperatures much longer recombination times can be expected. These long recombination times hold for lightly doped material. There are indications that dopants or other foreign elements may act as recombination centers which can considerably speed up the recombination reaction, but no reliable data are available in this area. The D_I values so determined (and therefore indirectly also of C_I^{eq} via the known product $D_I C_I^{\mathrm{eq}}$) were found to diverge over many orders of magnitude [3, 39] and with I formation enthalpies from ~ 1 to 4 eV. This is clearly an unsatisfactory situation. The problem is further complicated by the observation that the measured effective diffusivity $D_{(I,V)}^{\mathrm{eff}}$ depends on the type of Si material used. In the experiments of Fahey et al. [18] the transport of oxidation-induced Si interstitials through epitaxially-grown Si layers was much faster than through equally thick layers of as grown float-zone (FZ) or Czochralski (CZ) Si. This difference has been attributed to the presence of vacancy-type agglomerates left from the crystal growth process which might not be present in epitaxial Si layers. These vacancy agglomerates would have to be consumed by the injected I before further spread of interstitials can occur.

Nonetheless, considering the recent development involving several different categories of studies, we can now tentatively conclude that the migration enthalpies of vacancies and self-interstitials in silicon, h_V^{m} and h_I^{m} respectively, are relatively small while their formation enthalpies, h_V^{f} and h_I^{f} respectively, are large. This means that the V and I are moving fairly fast while their thermal equilibrium concentrations are fairly small. The most probable value of h_V^{m} is ~ 0.5–$1\,\mathrm{eV}$ while that of h_I^{m} is $\sim 1\,\mathrm{eV}$, and the corresponding most probable values of h_V^{f} is $\sim$ 3.5–3 eV while that of h_I^{f} is $\sim 4\,\mathrm{eV}$. Sinno et al. [40] used values of 0.457 and 0.937 eV respectively for h_V^{m} and h_I^{m} to satisfactorily model the formation of swirl defects (interstitial-type dislocation loops and vacancy-type clusters) in FZ Si, including the defect location, density, size, and their dependence on the crystal growth rate and the thermal gradient. Plekhanov et al. [41] used a h_V^{f} value of $\sim$ 3–3.4 eV to satisfactorily model the formation of voids in large diameter CZ Si. Moreover, in fitting the C and B diffusion results of Rücker et al. [33], as shown in Fig. 4.10, Scholz et al. [32] also needed to use h_I^{m} and h_V^{m} values smaller than 1 eV. This knowledge is consistent with recent quantum mechanical calculations which yielded fairly high h_I^{f} and h_V^{f} values and correspondingly low h_V^{m} and h_I^{m} values [42–46]. With the present estimates, it becomes also possible to connect in a reasonable and consistent way the fairly high diffusivities of native point defects found after low temperature electron irradiation [47] with the much lower apparent diffusivities which appear to be required to explain high-temperature diffusion experiments.

4.3.6 Oxygen and Hydrogen Diffusion

Oxygen is the most important electrically inactive impurity element in Si. In CZ Si, O is incorporated from the quartz crucible and usually present in concentrations in the order $10^{24}\,\mathrm{m}^{-3}$. An O atom in Si occupies the bond-centered interstitial position of two Si atoms and forms covalent bonds with the two Si atoms. Hence, its diffusion requires the breaking of bonds. The diffusivity of interstitial oxygen, $\mathrm{O_i}$, has been measured between about 300°C and the melting point of Si and is in good approximation described by

$$D_{\mathrm{i}} = 0.07 \exp(-2.44\,\mathrm{eV}/k_{\mathrm{B}}T)\,\mathrm{m}^2\mathrm{s}^{-1}\,. \tag{4.33}$$

The solubility $C_{\mathrm{i}}^{\mathrm{eq}}$ of interstitial O has been determined to be

$$C_{\mathrm{i}}^{\mathrm{eq}} = 1.53 \times 10^{27} \exp(-1.03\,\mathrm{eV}/k_{\mathrm{B}}T)\,\mathrm{m}^{-3}\,. \tag{4.34}$$

Since in most CZ Si crystals the grown-in $\mathrm{O_i}$ concentration exceeds $C_{\mathrm{i}}^{\mathrm{eq}}$ at typical processing temperatures, $\mathrm{O_i}$ precipitation will occur in the interior but not the surface regions (because of Oi out-diffusion) of CZ Si. This leads to the important technological application of intrinsic gettering [48] for improving the junction leakage and MOS capacitor charge holding time characteristics

of integrated circuit devices fabricated using CZ Si, which is not available to FZ Si.

Around 450°C O_i forms electrically active agglomerates, called thermal donors [49]. The formation kinetics of these agglomerates appears to require a fast diffusing species, for which both Si I [50] and molecular oxygen have been suggested [51]. The question of molecular oxygen in Si has not yet been settled.

Hydrogen plays an increasingly important role in silicon device technology because of its capability to passivate electrically active defects. The passivation of dislocations and grain boundaries is especially important for inexpensive multicrystalline Si used for solar cells. Both acceptors and donors can be passivated by H which is usually supplied to Si from a plasma. H in Si is assumed to diffuse as unbounded i atom in either a neutral or a positively charged form. The diffusivity of H in Si has been measured by Van Wieringen and Warmoltz [52] between 970 and 1200°C, see Fig. 4.1. Between room temperature and 600°C H diffusivities much lower than those extrapolated from the high-temperature data have been measured. Corbett and co-workers [53] rationalized this observation by suggesting that atomic H may form interstitially dissolved, essentially immobile H_2 molecules. Apparently, these molecules can then form plate-like precipitates [54]. As in the case of oxygen, the existence of H molecules has not been proven experimentally.

4.4 Diffusion in Germanium

Germanium has lost its leading role for electronic devices about four decades ago and is now mainly used as a detector material or in Si/Ge superlattices. Therefore, basically no papers have recently been published on diffusion in Ge. Another reason might be that diffusion in Ge can be consistently explained in terms of V-related mechanisms and no I contribution has to be invoked.

Figure 4.11 shows the diffusivities of group III and V dopants and of Ge in Ge as a function of inverse absolute temperature under intrinsic conditions. The doping dependence of dopant diffusion can be explained by one kind of acceptor-type native point defect. These native point defects have been assumed to be V since the earliest studies of diffusion in Ge [1], but a convincing experimental proof has only been given in 1985 by Stolwijk et al. based on the diffusion behavior of Cu in Ge [55].

Copper diffuses in Ge via an i-s mechanism [6]. In analogy to the case of Au and Pt in Si, its diffusion behavior may be used to check diffusion profiles for any indication of an I contribution via the KO mechanism. A concentration profile of Cu diffusion into a germanium wafer is shown in Fig. 4.12 [55]. The dashed U-shaped profile which is typical for the kickout mechanism obviously does not fit the experimental data. In contrast, the experimental profiles may

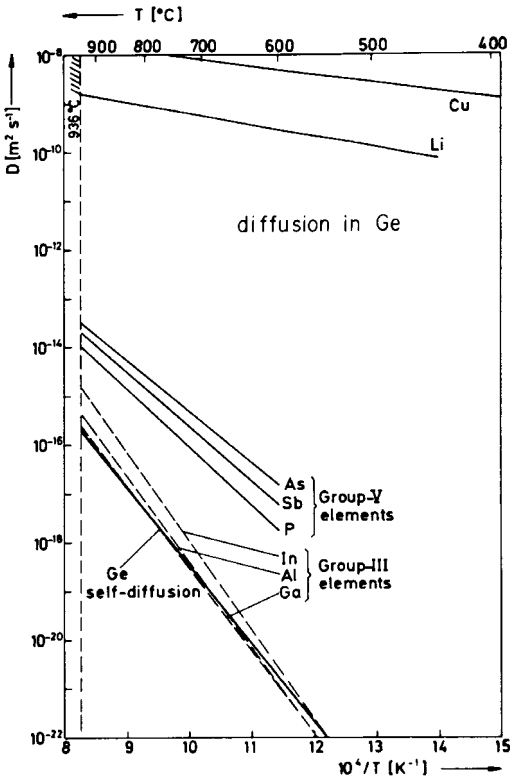

Fig. 4.11. Diffusivities of various elements (including Ge) in Ge as a function of inverse absolute temperature [4].

be well described by the constant diffusivity $D^{\text{eff}}_{(I,V)}$ given by (4.13). Values of the vacancy contribution to Ge self-diffusion

$$D_V C_V^{\text{eq}} = 21.3 \times 10^{-4} \exp(-3.11\,\text{eV}/k_\text{B}T)\,\text{m}^2\text{s}^{-1}\,, \tag{4.35}$$

as determined from Cu diffusion profiles, agree well with those measured from tracer self-diffusion in Ge [3,55]. The kind of excellent agreement shows that any Ge I contribution to the Ge self-diffusion process is negligible and hence Ge self-diffusion appears to be entirely governed by V. It is unclear why I play such an important role in diffusion processes in Si but no noticeable effect in Ge.

4.5 Diffusion in Gallium Arsenide

Gallium arsenide is the most important base material used for optoelectronic applications with diffusion processes essential in fabricating the devices. Self-diffusion and diffusion of dopant and other important impurity species in GaAs (and in other compound semiconductors) are governed by native point

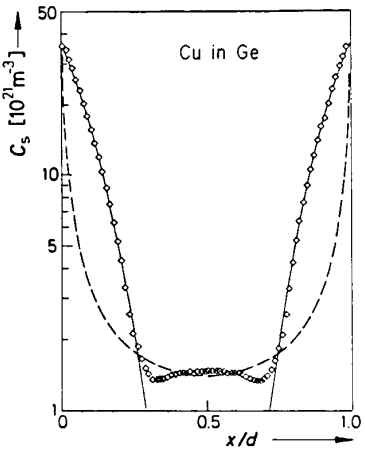

Fig. 4.12. Concentration profiles of Cu into a dislocation-free Ge wafer after diffusion for 15 minutes at 878°C. The solid line holds for the Frank-Turnbull and the dashed line for the kickout mechanism. From [55].

defects. Compared to that in Si, diffusion in GaAs exhibits a much more prominent dependence on the Fermi-level effect, and it also shows a dependence on the pressure of an As vapor phase. Moreover, the number of participating point defect species is more than that in Si. Vacancy, interstitialcy, as well as i-s diffusion mechanisms are involved. Detailed reviews can be found elsewhere [3, 56, 57].

4.5.1 Native Point Defects and General Aspects

The compound semiconductor GaAs has a thermodynamically allowed equilibrium composition range around the $Ga_{0.5}As_{0.5}$ composition. In thermal equilibrium coexistence with a GaAs crystal, there are four vapor phase species: Ga_1, As_1, As_2, and As_4. In the crystal, there are six single point defect species: vacancies of the Ga and As sublattices (V_{Ga} and V_{As}), self-interstitials of Ga and As (I_{Ga} and I_{As}), and antisite defects of a Ga atom on an As sublattice site (GaAs) and of an As atom on a Ga sublattice site (As_{Ga}). Any two single point defect species can form a paired species. There is no convincing evidence of the involvement of paired point defects in diffusion processes in GaAs, and the role of paired point defect species will not be considered here. The sum of the thermal equilibrium concentrations of the point defects constitutes the allowed GaAs crystal composition variation within its thermodynamically allowed range. For instance, considering the contributions of only the single point defects, the excess As concentration (δC_{As}) is given by

$$\delta C_{As} = \left[C^{eq}_{I_{As}} + C^{eq}_{As_{Ga}} - C^{eq}_{V_{As}}\right] - \left[C^{eq}_{I_{As}} + C^{eq}_{Ga_{As}} - C^{eq}_{V_{Ga}}\right] , \qquad (4.36)$$

while $\delta C_{Ga} = -\delta C_{As}$ is the excess Ga concentration, which is responsible for the compound crystal composition deviation from the $Ga_{0.5}As_{0.5}$ stoichiometry. In (4.36), the C are the various thermal equilibrium concentrations of

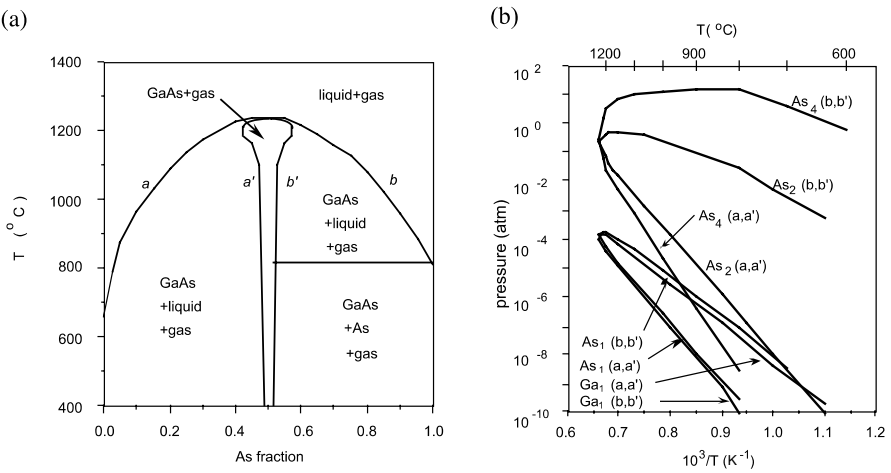

Fig. 4.13. (**a**) The schematic phase diagram of GaAs, with the thermodynamically allowed GaAs crystal composition range greatly exaggerated. (**b**) Partial pressures of the Ga and As vapor phases in equilibrium with the most gallium rich GaAs (a,a′) or the most arsenic rich GaAs (b,b′) [58].

the appropriate point defect species. Here the concentration of a point defect species includes those in all charge states.

Clearly, the following three categories of quantities form a mutual dependence, each of which may be regarded as the cause for the other two: (i) the vapor phase pressures; (ii) the GaAs crystal composition; and (iii) the point defect concentrations of the crystal.

To analyze experiments, it is convenient to regard the vapor phase pressure as the cause and the other quantities as consequences. For III-V compounds, the group V element vapor phase pressure are large, e.g., P_{As_4} and/or P_{As_2}, and can be readily measured. Figure 4.13a shows the GaAs phase diagram and Fig. 4.13b shows the vapor phase pressures [58]. Thus, for GaAs, according to the pressure effect,

$$C^{\mathrm{eq}}_{I^0_{\mathrm{As}}} \propto 1/C^{\mathrm{eq}}_{V^0_{\mathrm{As}}} \propto C^{\mathrm{eq}}_{V^0_{\mathrm{Ga}}} \propto 1/C^{\mathrm{eq}}_{I^0_{\mathrm{Ga}}} \propto (P_{\mathrm{As}_4})^{1/4} \tag{4.37}$$

holds for the four mobile point defect species in the neutral state. For GaAs, explicit expressions for the thermal equilibrium concentrations of all neutral single point defects have been obtained [59]. Such expressions should also be applicable to other III-V semiconductors.

Diffusion of many elements in GaAs have been investigated, with most of the studies focused on p-type dopants Zn and Be, on n-type dopants Si and Se, and on Cr which is used for producing semi-insulating GaAs. Since Zn, Be, Cr and a number of other elements diffuse via an i-s mechanism, this type of diffusion mechanism has historically received much more attention in GaAs than in Si and Ge. Similarly as for Si and Ge, it had been assumed for

a long time that only vacancies need to be taken into account to understand diffusion processes in GaAs, see the book of Tuck [60].

The compilation of earlier diffusion data in GaAs may be found elsewhere [60]. Only a few studies of self-diffusion in GaAs are available, but with advances in growing GaAs/AlAs-type superlattices using molecular beam epitaxy (MBE) or metalorganic chemical vapor deposition (MOCVD) methods, Al has served as an important foreign tracer element for elucidating Ga self-diffusion mechanisms. The observation that high-concentration Zn diffusion into a GaAs/$Al_xGa_{1-x}As$ superlattice leads to a dramatic increase in the Al-Ga interdiffusion coefficient [61] opened up the possibility to fabricate laterally structured optoelectronic devices by locally disordering superlattices. This dopant-enhanced superlattice disordering is a general phenomena occuring for other p-type dopants, e.g., Mg, and for n-type dopants, e.g., Si, Se and Te [57, 58]. The dopant-enhanced superlattice disordering also has helped to unravel the contributions of I and V to self- and dopants diffusion processes in GaAs. These superlattices with their typical period of about 10 nm allow one to measure Al-Ga interdiffusion coefficients, which turned out to be close to the Ga self-diffusion coefficient, down to much lower values than had been previously possible for Ga self-diffusion in bulk GaAs using radioactive Ga tracer atoms. The dependence of diffusion processes on the As vapor pressure has helped in establishing the role of self-interstitials versus vacancies.

The diffusivity of a substitutional species in GaAs generally shows a dependence on P_{As_4}, because the concentration of the responsible point defect species is dependent upon P_{As_4}, (4.37). The diffusivity will also exhibit a dependence on doping because of the involvement of charged point defects whose concentration is influenced via the Fermi-level effect. Furthermore, non-equilibrium concentrations of native point defects may be induced by the in-diffusion of dopants such as Zn starting from a high surface concentration. Much less is known on the diffusion processes of atoms dissolved on the As sublattice, but recent experiments indicate the dominance of As I on the diffusion of the isoelectronic group V element N [62], P and Sb [63–65], and the group VI n-type dopant S [66]. These results imply also the dominance of As I on As self-diffusion, which is in contrast to the earlier As self-diffusion results of Palfrey et al. [67] favoring the dominance of As V.

4.5.2 Gallium Self-Diffusion and Superlattice Disordering

Intrinsic Gallium Arsenide

The self-diffusion coefficient $D_{Ga}(n_i)$ of Ga in intrinsic GaAs has been measured by Goldstein [68] and Palfrey et al. [69] using radioactive Ga tracer atoms. This method allows measurements of $D_{Ga}(n_i)$ down to about $10^{-19}\,m^2/s$. Measurements of the interdiffusion of Ga and Al in GaAs/$Al_xGa_{1-x}As$ superlattices extended the range to much lower values [70–74].

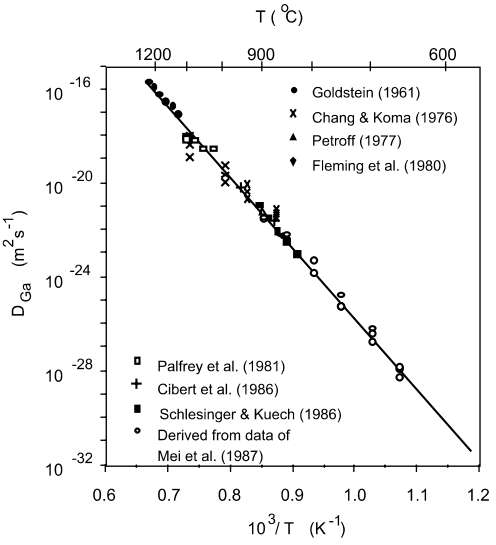

Fig. 4.14. Plot of available data on Ga self-diffusion in GaAs and data on Ga/Al interdiffusion in GaAs/AlGaAs superlattices under intrinsic conditions together with D_{Ga} derived [75] from the data of Mei et al. [87].

The various data points have been approximately fitted by Tan and Gösele [75, 76] to the expression

$$D^V_{\mathrm{Ga}}(n_{\mathrm{i}}, 1\,\mathrm{atm}) \approx 2.9 \times 10^4 \exp(-6\,\mathrm{eV}/k_{\mathrm{B}}T)\,\mathrm{m^2 s^{-1}}\,, \qquad (4.38)$$

see Fig. 4.14. Equation (4.38) is valid for the As_4 pressure of 1 atm or for GaAs crystals with compositions at the As-rich boundary shown in Fig. 4.13a, and the superscript V in the quantity D^V_{Ga} specifies that the quantity is due to the Ga sublattice V contribution to Ga self-diffusion. This is because, at ~ 1 atm, the disordering rate of the GaAs/Al_xGa_{1-x}As superlattices increases as the ambient As_4 pressure is increased [77, 78]. The corresponding D^V_{Ga} values for GaAs crystals at the Ga-rich boundary is then

$$D^V_{\mathrm{Ga}}(n_{\mathrm{i}}, \text{Ga-rich}) \approx 3.93 \times 10^8 \exp(-7.34\,\mathrm{eV}/k_{\mathrm{B}}T)\,\mathrm{m^2 s^{-1}}\,. \qquad (4.39)$$

For (4.38) and (4.39), it turned out that the responsible vacancy species is the triply-negatively-charged Ga vacancies V^{3-}_{Ga}, to be discussed in the next paragraph. However, the Al-Ga interdiffusion coefficient also increases for very low arsenic vapor pressures [77, 78], indicating that D_{Ga} is governed by Ga I for sufficiently low As vapor pressures [57]. The role of Ga V and I will become clearer when Ga diffusion in doped GaAs/Al_xGa_{1-x}As superlattices is considered and when diffusion of the p-type dopant Zn and Be is considered. Combining the Al-Ga interdiffusion data of Hsieh et al. [79] obtained under Ga-rich ambient conditions, and the deduced Ga self-diffusion coefficients from analyzing Zn diffusion [80] and Cr diffusion [81], Tan et al. [82] summarized that

$$D^I_{\mathrm{Ga}}(n_{\mathrm{i}}, \text{Ga-rich}) \approx 4.46 \times 10^{-8} \exp(-3.37\,\mathrm{eV}/k_{\mathrm{B}}T)\,\mathrm{m^2 s^{-1}} \qquad (4.40)$$

holds for the Ga I contribution to Ga self-diffusion in GaAs crystals with composition at the Ga-rich boundary shown in Fig. 4.13a. The corresponding values for GaAs crystals with composition at the As-rich boundary shown in Fig. 4.13a is then

$$D^I_{\mathrm{Ga}}(n_{\mathrm{i}}, 1\,\mathrm{atm}) \approx 6.05 \times 10^{-4} \exp(-4.71\,\mathrm{eV}/k_{\mathrm{B}}T)\,\mathrm{m^2 s^{-1}}\,. \tag{4.41}$$

For (4.40) and (4.41), it turned out that the responsible point defect species is the doubly-positively-charged Ga self-interstitials I^{2+}_{Ga}, as will be discussed in Sect. 4.5.2.

However, as has been first noticed by Tan et al. [83], under intrinsic conditions, for a number of Al-Ga interdiffusion studies [70, 84, 85] and two recent Ga self-diffusion studies using stable Ga isotopes [83, 86], the results are fitted better by

$$D_{\mathrm{Ga}}(n_{\mathrm{i}}, 1\,\mathrm{atm}) \approx 4.3 \times 10^{-3} \exp(-4.24\,\mathrm{eV}/k_{\mathrm{B}}T)\,\mathrm{m^2 s^{-1}} \tag{4.42}$$

instead of by (4.38). Figure 4.15 shows the values per (4.38) and (4.42) and the associated data. There has yet to be a satisfactory explanation of the discrepancy between these expressions. On the one hand, (4.42) does offer a better fit to the more recent data, but on the other, it does not seem to be consistent with the Al-Ga data of Mei et al. [87] under Si doping which are associated with a 4 eV activation enthalpy. In accordance with the Fermi-level effect, the Ga diffusion activation enthalpy decreases by about 2 eV in n-doped materials [57], which would mean that (4.38) is more reasonable. A number of reasons, however, could affect the accuracy of the experimental results. These will include accidental contamination by n-type dopants in the nominal intrinsic materials, band off-sets in the case of Al-Ga interdiffusion, and the fact that the materials did not have the As-rich composition to start with and the experimental temperature-time was not sufficient to change the materials into As-rich for most part of the experimental time.

Doped Gallium Arsenide

No studies of Ga self-diffusion in doped bulk GaAs have been reported, but a wealth of data on Al-Ga interdiffusion in both n-type and p-type doped GaAs/$\mathrm{Al_xGa_{1-x}As}$ superlattices is available. These interdiffusion experiments were triggered by the observation of Zn in-diffusion enhanced superlattice disordering due to Laidig et al. [61]. A number of disordering mechanisms have been proposed [61, 88–90] for a particular dopant, but none is general enough to account for the occurrence of an enhanced Al-Ga interdiffusion rate for also other dopants. The observed dopant enhanced interdiffusion appears to be due to two main effects [75, 76]: (i). The thermal equilibrium concentration of appropriately charged point defects is enhanced by doping, i.e., the Fermi-level effect. In the case of the n-type dopant Si, mainly the *presence* of the dopant is of importance, but not its movement. Compensation

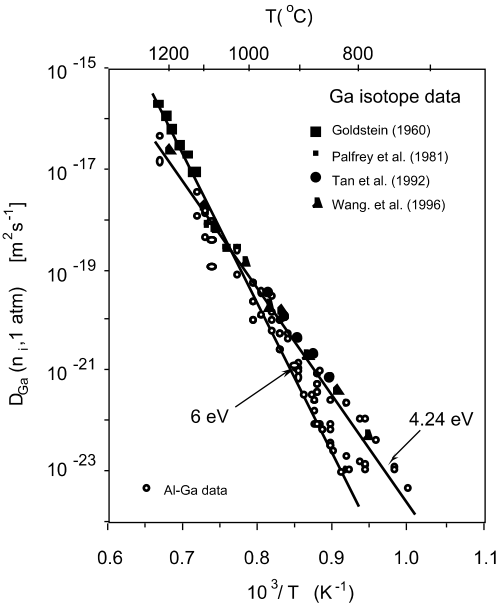

Fig. 4.15. Data and fitting lines for the intrinsic Ga or Al-Ga diffusivity under 1 atm of As_4 pressure. The 6 eV line is that given by (4.38) and the 4.24 eV line that given by (4.42). All Ga data are directly measured ones using norminaly intrinsic GaAs. The Al-Ga data include directly measured ones using norminaly intrinsic $GaAs/Al_xGa_{1-x}As$ superlattices as well as those deduced [75] from the Mei et al. data [87] obtained using Si doped $GaAs/Al_xGa_{1-x}As$ superlattices.

doping, e.g. with Si and Be, should not lead to enhanced Al-Ga interdiffusion, in agreement with experimental results [91, 92]. (ii) For a dopant with high diffusivity and solubility, *non-equilibrium native point defects* are generated.

Depending on whether a supersaturation or an undersaturation of point defects develops, the enhanced disordering rate due to the Fermi level effect may be further increased or decreased. Irrespective of the starting material composition, such non-equilibrium native point defects drive the dopant diffused region crystal composition first toward an appropriate allowed GaAs crystal composition limit shown in Fig. 4.13a. When the super- or undersaturation of point defects becomes so large that the crystal local region exceeded the allowed composition limit, extended defects form to bring the composition of the region back to that composition limit. Afterwards, this permits the diffusion processes to be described by an equilibrium point defect process appropriate for the crystal local region which is at an appropriate allowed composition limit. The crystal is in a non-equilibrium state because of the spatially changing composition. The diffusion of high-concentration Zn and Be in GaAs [80, 93] and their effects on $GaAs/Al_xGa_{1-x}As$ superlattices [94] appear to be such cases. Interdiffusion of Al-Ga in *n-type* GaAs/AlAs su-

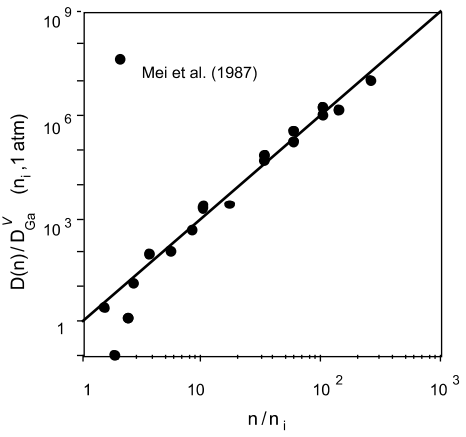

Fig. 4.16. The $(n/n_\mathrm{i})^3$ dependence of the Al-Ga interdiffusion data of Mei et al. [87], with $D^V_\mathrm{Ga}(n_\mathrm{i}, 1\,\mathrm{atm})$ given by (4.38). The data cannot be analyzed to a similar degree of satisfaction via the use of (4.42) to a power law dependence on n/n_i. Redrawn from [75].

perlattices will be first discussed. This concerns with the case of Si-doped GaAs which allows to identify the type and the charge state of the native point defect dominating Ga self-diffusion in n-type GaAs. In Fig. 4.16, the enhanced Al-Ga interdiffusion coefficients under Si-doping are plotted in a normalized form as a function of n/n_i of the appropriate temperature. These data, obtained by Mei et al. [87], show a clear doping dependence [75, 76]

$$D_{\mathrm{Al-Ga}}(n, 1\,\mathrm{atm}) = D_\mathrm{Ga}(n_\mathrm{i}, 1\,\mathrm{atm})[n/n_\mathrm{i}]^3 \tag{4.43}$$

with $D^V_\mathrm{Ga}(n_\mathrm{i}, 1\,\mathrm{atm})$ given by (4.38). Equation (4.43) indicates the involvement of a triply-negatively-charged native point defect species. Based on the pressure dependence of the interdiffusion coefficient of n-doped superlattices [56, 78] this defect has to be the gallium vacancy V^{-3}_Ga, as predicted by Baraff and Schlüter [95]. Values of $D^V_\mathrm{Ga}(n_\mathrm{i}, 1\,\mathrm{atm})$ calculated from the Mei et al. data and shown in Fig. 4.14 are in good agreement with values extrapolated from higher temperatures. Thus, including the As vapor pressure dependence, we may write the Ga self-diffusion coefficient in n-type GaAs as

$$D_\mathrm{Ga}(n, P_{\mathrm{As_4}}) = D^V_\mathrm{Ga}(n_\mathrm{i}, 1\,\mathrm{atm})[n/n_\mathrm{i}]^3[P_{\mathrm{As_4}}]^{1/4} \tag{4.44}$$

where $D^V_\mathrm{Ga}(n_\mathrm{i}, 1\,\mathrm{atm})$ is given by (4.38). The much later claim that these Si-doping induced Al-Ga interdiffusion data show a quadratic dependence on n [96] is erroneous, because of the use of the room temperature n_i value as that for high temperature ones by the authors. Furthermore, the statement that there is no Fermi-level effect [97] bears little credence, for it is based on Al-Ga interdiffusion results with extremely low Si doping, which are threshold phenomena that may be influenced by many other uncontrolled factors. Tellurium-doped GaAs based superlattices show a weaker dependence of the Al-Ga interdiffusion coefficient on the Te concentration than expected from (4.44) [98], especially at very high concentrations. The probable cause is that,

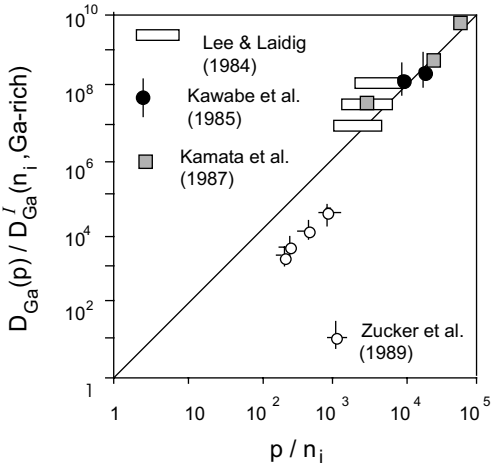

Fig. 4.17. Fits of some of the available p-dopant enhanced Al-Ga interdiffusion data, with $D^I_{\rm Ga}(n_{\rm i}, \text{Ga-rich})$ given by (4.40). The data exhibit an approximately quadratic dependence on $p/n_{\rm i}$, indicating that the dominant native point defect is $I^{2+}_{\rm Ga}$. From [94].

due to clustering, not all Te atoms are electrically active to contribute to the electron concentration [99].

The available Al-Ga interdiffusion data in *p-type* GaAs based superlattices [61, 91, 100–104] had been first thought to be not analyzable in a manner analogous to that done for the n-doping effect [75, 76]. As shown in Fig. 4.17, however, some of these data has been later approximately fitted by [94]

$$D_{\rm Al-Ga}(p, \text{Ga-rich}) = D^I_{\rm Ga}(n_{\rm i}, \text{Ga-rich})[p/n_{\rm i}]^2 \tag{4.45}$$

where $D^I_{\rm Ga}(n_{\rm i}, \text{Ga-rich})$ is given by (4.40). Equation (4.45) shows that the dominant native point defects under p-doping to a sufficient concentration are $I_{\rm Ga}$ species, and the p^2 dependence of $D_{\rm Al-Ga}(p, \text{Ga-rich})$ shows that the $I_{\rm Ga}$ are doubly-positively-charged. The data shown in Fig. 4.17 [91, 100, 103, 104] are those under the dopant *in-diffusion* conditions, while the rest are those under the dopant *out-diffusion* conditions involving grown-in dopants without an outside dopant source. Under out-diffusion conditions, the dopant diffusivity values are too small to be reliably measured. The fit shown in Fig. 4.17 is seemingly satisfactory but nowhere near that for the Si-doping case (Fig. 4.16). Even if the fit were perfect, the essential native point defect equilibrium situation implied by Fig. 4.17 is only an apparent phenomenon, for it applies only to the p-dopant diffusion front region while the whole crystal is having a spatially varying composition. This point is most obvious in the data of Lee and Laidig [100] which were obtained in a high As_4 vapor pressure ambient.

The grossly different results for in- and out-diffusion conditions is due to non-equilibrium concentrations of native point defects induced by high-concentration diffusion of Zn or Be. Both Zn and Be diffuse via an i-s mechanism as will be discussed in more detail in the subsequent section. Historically, most authors [60] considered that diffusion of p-type dopants is governed by

the Longini mechanism [105] involving Ga vacancies

$$A_i^+ + V_{Ga}^0 \Leftrightarrow A_s^- + 2h\,, \tag{4.46}$$

where h is a hole and the interstitial species of the dopant is assumed to be positively charged, A_i^+. The Longini mechanism is the same as the FT mechanism, except it deals with charged species. The superlattice disordering results indicate that for these dopants, the KO mechanism [106] involving Ga self-interstitials

$$A_i^+ \Leftrightarrow A_s^- + I_{Ga}^{2+} \tag{4.47}$$

is operating instead. This also indicates that Ga self-diffusion is governed by Ga I under p-doping conditions. Within the framework of the kickout mechanism the dopant in-diffusion generates a supersaturation of I_{Ga} with a corresponding increase of dopant diffusion and the Ga self-diffusion component involving Ga I. Because of the I_{Ga} supersaturation, the dopant diffused region tends toward the Ga-rich composition. In the case of Zn in-diffusion to very high concentrations, it will be discussed in detail that the I_{Ga} supersaturation is so large that in a small fraction of the diffusion time extended defects form [93, 107], resulting in that the Zn diffused region composition is at the thermodynamically allowed Ga-rich composition limit, and is associated with the appropriate thermal equilibrium point defect concentrations. This is the reason for the satisfactory fit shown in Fig. 4.17.

In the case of grown-in dopants without an outside source the KO mechanism involves the consumption of I_{Ga} which leads to an I_{Ga} undersaturation with a corresponding decrease in dopant diffusion [108–111] and the Ga self-diffusion component involving I_{Ga}. The results of the superlattice disordering experiments are consistent with the expectations based on the KO mechanism. In contrast, the Longini mechanism predicts an undersaturation of V for in-diffusion conditions and a supersaturation for out-diffusion conditions with a corresponding decrease and increase of a V dominated Ga self-diffusion component, respectively. Since the predictions based on the Longini mechanism are just opposite to the observed superlattice disordering results, it can be concluded that: (i) Zn diffusion occurs via the KO mechanism, and (ii) Ga self-diffusion in p-type GaAs is governed by I_{Ga}.

In contrast to the group II acceptors Zn and Be, the group IV acceptor carbon (C) occupying the As sublattice sites diffuses slowly. This allows the native point defects to be maintained at their thermal equilibrium values. The effect of C on the disordering of GaAs/$Al_xGa_{1-x}As$ superlattices [112] is described well by

$$D_{Al-Ga}^{eq} = D_{Ga}^{I}(n_i)[p/n_i]^2\,, \tag{4.48}$$

where $D_{Ga}^{I}(n_i)$ is given by (4.40) and (4.41) respectively for data obtained under Ga-rich and As-rich ambient conditions.

The pressure dependence of disordering of p-doped superlattices confirms the predominance of Ga I in Ga self-diffusion [56]. The magnitude of the

enhancement effect, its restriction to the dopant-diffused region and the implantation results of Zucker et al. [104] indicate that a Fermi level effect has to be considered in addition to non-equilibrium point defects.

Combining the results for the p-type and the n-type dopant induced disordering including an I supersaturation s_I defined as $s_I = C_I(n(p))/C_i^{\mathrm{eq}}(n(p))$, and an analogous V supersaturation s_V defined as $s_V = C_V(n(p))/C_V^{\mathrm{eq}}(n(p))$, where $(n(p))$ indicates doping conditions, we may express the Ga self-diffusion coefficient approximately as

$$D_{\mathrm{Ga}}\,(n(p), P_{\mathrm{As_4}}) = D^I_{\mathrm{Ga}}(n_{\mathrm{i}}, 1\,\mathrm{atm})[p/n_{\mathrm{i}}]^2 P^{-1/4}_{\mathrm{As_4}} s_I + D^V_{\mathrm{Ga}}(n_{\mathrm{i}}, 1\,\mathrm{atm})[n/n_{\mathrm{i}}]^3 P^{1/4}_{\mathrm{As_4}} s_V\,. \tag{4.49}$$

In (4.49) the quantities $D^V_{\mathrm{Ga}}(n_{\mathrm{i}}, 1\,\mathrm{atm})$ and $D^I_{\mathrm{Ga}}(n_{\mathrm{i}}, 1\,\mathrm{atm})$ are given respectively by (4.38) and (4.41). In writing down (4.49), the As-rich GaAs, designated by $P_{\mathrm{As_4}} = 1\,\mathrm{atm}$, is chosen as the reference material state, and with GaAs crystals of all other compositions represented by an appropriate $P_{\mathrm{As_4}}$ value. Equation (4.49) describes all presently known essential effects on $\mathrm{GaAs/Al_xGa_{1-x}As}$ superlattice disordering. In the case of non-equilibrium Ga V injected by a Si/As cap [113], $s_V > 0$ holds. In the case of ion-implantation, both $s_I > 0$ and $s_V > 0$ may hold and both quantities will be time dependent. In the case of diffusion-induced non-equilibrium point defects the presence of dislocations will allow local equilibrium between intrinsic point defects to establish in the two sublattices. In this way a large supersaturation of I_{Ga} in the Ga sublattice may lead to an undersaturation of I_{As} or a supersaturation of V_{As} in the As sublattice.

4.5.3 Arsenic Self-Diffusion and Superlattice Disordering

Since there is only one stable As isotope, ^{75}As, As self-diffusion in GaAs cannot be studied using stable As isotopes. In intrinsic GaAs, however, three arsenic self-diffusion studies have been conducted using radioactive tracers [62, 63, 67]. In the experiment of Palfrey et al. [67], the $\mathrm{As_4}$ pressure dependence of As self-diffusion indicated that V_{As} may be the responsible native point-defect species. This is, however, in qualitative contradiction to the conclusion reached recently from a large number of studies involving As atoms and other group V and VI elements that the responsible native point-defect species should be I_{As}. The latter studies include: (i) As-Sb and As-P interdiffusion in intrinsic $\mathrm{GaAs/GaSb}_x\mathrm{As}_{1-x}$ and $\mathrm{GaAs/GaP}_x\mathrm{As}_{1-x}$ type superlattices for which x is small so as to avoid a large lattice mismatch [63–65]; (ii) P and Sb in-diffusion into GaAs under appropriate P and As pressures so as to avoid extended defect formation which leads to complications [63–65]; (iii) an extensive analysis of the S in-diffusion data in GaAs [66]; (iv) out-diffusion of N from GaAs [62]. A plot of the relevant data is shown in Fig. 4.18, from which the lower limit of the As self-diffusion coefficient, assigned to be due to the As self-interstitial contribution, is determined to be

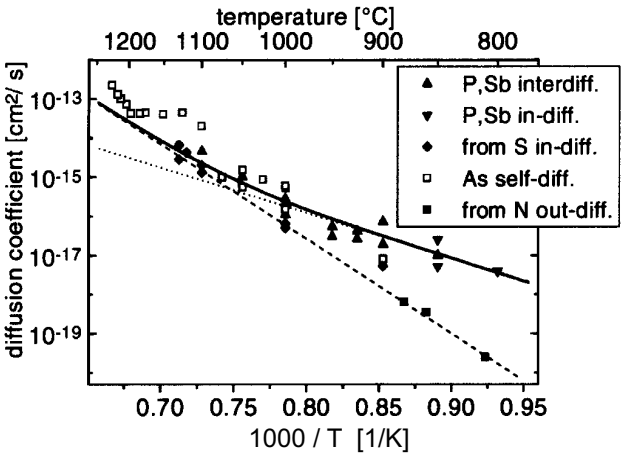

Fig. 4.18. Data on As self-diffusion coefficient, obtained using radioactive As tracers (open squares), the group V elements N, P, and Sb and the group VI donor S (filled symbols). The dashed fitting line is given by (4.50), and the solid line is a better overall fitting. From [64].

$$D^I_{\mathrm{As}}(n_{\mathrm{i}}, 1\,\mathrm{atm}) \approx 6 \times 10^{-2} \exp(-4.8\,\mathrm{eV}/k_{\mathrm{B}}T)\,\mathrm{m^2 s^{-1}}\,. \tag{4.50}$$

For P-As and Sb-As interdiffusion as well as P and Sb in-diffusion cases [63–65], the profiles are error function shaped. With P and Sb assumed to be i-s elements, such diffusion profiles are described by an effective diffusivity of the type

$$D^{\mathrm{eff}}_{\mathrm{s}} = D_{\mathrm{i}} C^{\mathrm{eq}}_{\mathrm{i}} / C^{\mathrm{eq}}_{\mathrm{s}} \tag{4.51}$$

under native point defect equilibrium conditions, which is satisfied by either the KO mechanism involving I_{As} or the Longini (or FT) mechanism involving V_{As}. The conclusion that I_{As} is the responsible species is reached for this group of experiments because the diffusion rate increases upon increasing the ambient As vapor pressure. I_{As} should be the responsible species in the N out-diffusion experiments [62] because the N profile is typical of that due to the KO reaction (4.47) under the condition of an I_{As} undersaturation, which is qualitatively different from those obtainable from the dissociative reaction (4.46). I_{As} should also be the responsible species in the S in-diffusion experiments because the S profile [66] is typical of that due to the KO mechanism reaction $\mathrm{S}^+_{\mathrm{i}} \Leftrightarrow \mathrm{S}^+_{\mathrm{s}} + I^0$ under the condition of an I_{As} supersaturation, which is also qualitatively different from those obtained from any possible reactions of the FT or Longini mechanisms. It is seen from Fig. 4.18 that the available As self-diffusion data lie close to those deduced from the P, Sb, N, and S studies, and it may thus be inferred that As self-diffusion has a component contributed by I_{As}.

There are yet no doping dependence studies using the isoelectronic group V elements N, P, and Sb, and hence the charge nature of the involved I_{As} has not yet been determined. However, S is a group VI donor occupying the As sublattice sites. In analyzing S in-diffusion [66], it was necessary to assume that neutral I_{As} species were involved, which is therefore a most likely species responsible for As self-diffusion.

There is also a study on the disordering of GaAs/$\mathrm{Al_xGa_{1-x}As}$ superlattices by the group IV acceptor species C [112] which occupy the As sublattice sites. While there is no information obtained from this study on As self-diffusivity, satisfactory descriptions of the C diffusion profiles themselves were obtained also with the use of a kickout reaction involving neutral As self-interstitials, discussed later. This lends further support to the interpretation that neutral As self-interstitials are responsible for As self-diffusion.

4.5.4 Impurity Diffusion in Gallium Arsenide

Silicon

For GaAs the main n-type dopant is Si. It is an amphoteric dopant mainly dissolved on the Ga sublattice but shows a high degree of self-compensation at high concentrations due to an increased solubility on the As sublattice.

The Si diffusivity shows a strong dependence on its own concentration, which had been modeled by a variety of mechanisms [113–115]. Apparently, Si diffusion is dominated by negatively charged V_{Ga} and that its apparent concentration dependence is actually a Fermi level effect. Results on Si diffusion into n-type (Sn-doped) GaAs confirm the Fermi level effect [115] and contradict the other models, e.g., the $\mathrm{Si_{Ga}}$-$\mathrm{Si_{As}}$ pair-diffusion model of Greiner-Gibbons [114]. In the Fermi-level effect model, Yu et al. [115] used mainly V_{Ga}^{3-} to fit the Si in-diffusion profiles, and more recently Chen et al. [116] found *only* V_{Ga}^{-3} is needed to fit these profiles. This is in consistency with the fact that V_{Ga}^{3-} dominating GaAs/AlAs superlattice disordering under n-doping conditions. In the work of Chen et al. [116] the Si source material and the GaAs crystal are regarded as forming a heterostructure so that electrical effects due to the heterojunction are also accounted for. In these analyses [115, 116], the diffusivity of the Si donor species $\mathrm{Si_{Ga}^{+}}$ satisfies

$$D_{\mathrm{Si}}(n) = D_{\mathrm{Si}}(n_{\mathrm{i}})(n/n_{\mathrm{i}})^3\,, \tag{4.52}$$

which indicates that V_{Ga}^{3-} governs the diffusion of $\mathrm{Si_{Ga}^{+}}$. Satisfactory fits of the experimental data of Greiner and Gibbons [114] and of Kavanagh et at. [113] were obtained using (4.51) with

$$D_{\mathrm{Si}}(n_{\mathrm{i}}) = 5.2\exp(-4.98\,\mathrm{eV}/k_{\mathrm{B}}T)\,\mathrm{m^2s^{-1}} \tag{4.53}$$

in the work of Yu et al. [115], while $D_{\mathrm{Si}}(n_{\mathrm{i}})$ values 10 times larger than that given by (4.53) were needed in the analysis of Chen et al. [116].

In a set of Si out-diffusion experiments, You et al. [117] found that the Si profiles also satisfy (4.52) but the needed $D_{\mathrm{Si}}(n_{\mathrm{i}})$ values are

$$D_{\mathrm{Si}}(n_{\mathrm{i}}, 1\,\mathrm{atm}) = 6.67 \exp(-3.91\,\mathrm{eV}/k_{\mathrm{B}}T)\,\mathrm{m^2 s^{-1}}\,, \tag{4.54}$$

$$D_{\mathrm{Si}}(n_{\mathrm{i}}, \mathrm{Ga\text{-}rich}) = 9.18 \times 10^4 \exp(-5.25\,\mathrm{eV}/k_{\mathrm{B}}T)\,\mathrm{m^2 s^{-1}}\,, \tag{4.55}$$

respectively, for experiments conducted under As-rich and Ga-rich ambient conditions.

The $D_{\mathrm{Si}}(n_{\mathrm{i}})$ expressed by (4.54) and (4.55) are larger than those of (4.53) by several orders of magnitude at temperatures above $\sim 800^{\circ}$C, which indicates the presence of an undersaturation and a supersaturation of V_{Ga}^{3-}, respectively, under the Si in- and out-diffusion conditions [117]. For the in-diffusion case, the starting GaAs crystal contains V_{Ga}^{3-} and the neutral Ga vacancies V_{Ga}^{0} to the thermal equilibrium concentrations of those of the intrinsic material. Upon in-diffusion of Si atoms, V_{Ga}^{3-} (and hence also V_{Ga}^{0}) become undersaturated relative to the thermal equilibrium V_{Ga}^{3-} concentration values appropriate for the n-doping conditions, which can only be alleviated via inflow of V_{Ga}^{3-} from the interface of the Si source material and the GaAs crystal. The reverse analogy holds for the Si out-diffusion case. Since V_{Ga}^{3-} diffusion should be much faster than that of the $\mathrm{Si}_{\mathrm{Ga}}^{+}$ atoms, in either case there shall be no substantial spatial variations in the distribution of the V_{Ga}^{0} species while the spatial distribution of V_{Ga}^{3-} follows the local n^3 value.

Diffusion of Interstitial-Substitutional Species

Carbon

The group IV element carbon (C) occupies the As sublattice sites in GaAs and is a shallow acceptor, designated as $\mathrm{C_s^-}$ to emphasize that it is most likely an i-s species. By in-situ doping during MBE crystal growth, $\mathrm{C_s^-}$ reaches high solubilities [118] and diffuses slowly [119], which are attractive features when compared to the main p-type dopants Zn and Be in GaAs. The measured $\mathrm{C_s^-}$ diffusivity values of a few groups obtained under As-rich annealing conditions [112, 118–122] are fitted well by the expression

$$D_{\mathrm{s}}(1\,\mathrm{atm}) = 4.79 \times \exp(-3.13\,\mathrm{eV}/k_{\mathrm{B}}T)\,\mathrm{m^2 s^{-1}}\,. \tag{4.56}$$

The corresponding Ds values under Ga-rich conditions should therefore be

$$D_{\mathrm{s}}(\mathrm{Ga\text{-}rich}) = 6.5 \times \exp(-4.47\,\mathrm{eV}/k_{\mathrm{B}}T)\,\mathrm{m^2 s^{-1}}\,. \tag{4.57}$$

These fits are shown in Fig. 4.19. In the work of You et al. [112] the $\mathrm{C_s^-}$ diffusivity data were obtained by the individual fittings of $\mathrm{C_s^-}$ profiles which are not quite error function shaped. In order to fit these profiles well, together with a carbon precipitation process, it was also necessary to use the kickout reaction

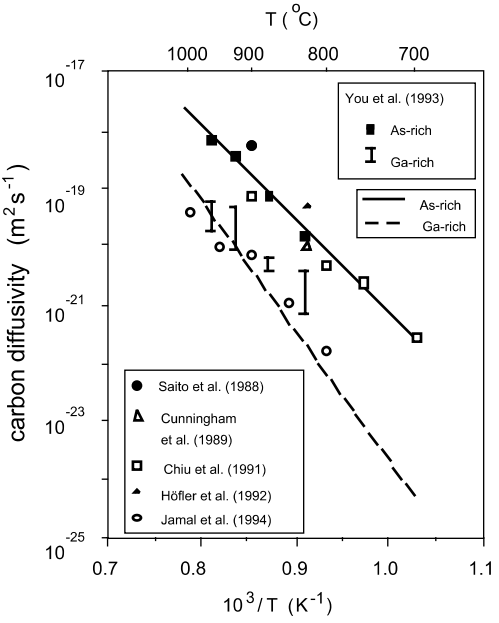

Fig. 4.19. Available carbon diffusivity data and fittings in GaAs. From [112].

$$C_s^- + I_{As}^0 \Leftrightarrow C_i^- , \tag{4.58}$$

where C_i^- is an interstitial C atom which is also assumed to be an acceptor, and I_{As}^0 is a neutral As self-interstitial. Later, Moll et al. [123] identified the nature of the precipitation process as that of graphite formation. The As self-interstitials are maintained at their thermal equilibrium values during C diffusion, because of the low diffusivity value of C.

Zinc and Beryllium

The main p-type dopants in GaAs based devices, Zn and Be, diffuse via an i-s mechanism in GaAs as well as in many other III-V compounds. In most works Zn and Be diffusion have been discussed in terms of the much earlier suggested FT or Longini mechanism [60], but only the KO mechanism involving I_{Ga} is quantitatively consistent with the superlattice disordering results as well as with Zn diffusion results [80, 93].

Isoconcentration diffusion of Zn isotopes in GaAs predoped by Zn showed error function profiles [124, 125] with the substitutional Zn diffusivity values of

$$D_s(p, 1\,\text{atm}) = D_s(n_i, 1\,\text{atm})(C_s/n_i)^2 \tag{4.59}$$

for As-rich GaAs and an analogous expression for Ga-rich GaAs. At sufficiently high Zn concentrations, since the GaAs hole concentration p equals approximately the Zn_s concentration ($p \sim C_s$), (4.59) shows that the responsible native point defect species can only be the doubly-positively-charged

Ga self-interstitials or vacancies, I_{Ga}^{2+} or V_{Ga}^{2+}. Under high-concentration Zn in-diffusion conditions, the GaAs/$Al_xGa_{1-x}As$ superlattices disordering rates are tremendously high, indicating the presence of a high supersaturation of the responsible point defects. Thus, the native point-defect species responsible for Zn diffusion, and also for Ga self-diffusion and Al-Ga interdiffusion under p-doping conditions, is I_{Ga}^{2+} according to reaction (4.47), and not V_{Ga}^{2+} according to reaction (4.46). In the latter case only an undersaturation of V_{Ga}^{2+} can be incurred by Zn in-diffusion which should then retard Al-Ga interdiffusion rates in superlattices, in contradiction with experimental results. In the Zn isoconcentration diffusion experiments, a non-equilibrium I_{Ga}^{2+} concentration is not involved. Similarly, for Zn diffusion to low concentrations below the n_i value, a non-equilibrium concentration of I_{Ga}^{2+} is also not present, and the Zn diffusivity values may be represented by that under the intrinsic conditions, $D_s(n_i)$. As analyzed by Yu et al. [80], Zn isoconcentration experiments and Zn in-diffusion experiments at high concentrations yielded the value range of

$$D_s(n_i, 1\,\text{atm}) = 1.6 \times 10^{-6} \exp(-2.98\,\text{eV}/k_BT)\,\text{m}^2\text{s}^{-1}\,, \quad (4.60a)$$

$$D_s(n_i, 1\,\text{atm}) = 9.68 \times 10^{-3} \exp(-4.07\,\text{eV}/k_BT)\,\text{m}^2\text{s}^{-1}\,. \quad (4.60b)$$

The two analogous expressions for Ga-rich materials are respectively

$$D_s(n_i, \text{Ga-rich}) = 1.18 \times 10^{-10} \exp(-1.64\,\text{eV}/k_BT)\,\text{m}^2\text{s}^{-1}\,, \quad (4.61a)$$

$$D_s(n_i, \text{Ga-rich}) = 7.14 \times 10^{-7} \exp(-2.73\,\text{eV}/k_BT)\,\text{m}^2\text{s}^{-1}\,. \quad (4.61b)$$

The values of (4.60ab) and (4.61ab) and the associated data are plotted in Fig. 4.20.

The correspondingly deduced I_{Ga}^{2+} contribution to Ga self-diffusion has been included in (4.38) and (4.39). Because of the lack of a proper Be source for in-diffusion studies, and in Be out-diffusion studies with Be incorporated using MBE or MOCVD methods the Be diffusivity is too small, there are no reliable Be diffusivity data.

Out-diffusion of Zn or Be in GaAs doped to fairly high concentrations during crystal is associated with a high I_{Ga}^{2+} undersaturation, leading to Zn or Be out-diffusion rates orders of magnitude smaller than those under in-diffusion conditions [109,110,126]. In-diffusion of high concentration Zn into GaAs induces an extremely large I_{Ga}^{2+} supersaturation, because the condition

$$D_i C_i^{eq} \gg D_{Ga}^{SD}(p) \quad (4.62)$$

holds. As first noted by Winteler [107], this I_{Ga}^{2+} supersaturation leads to the formation of extended defects. In recent works three kinds of extended defects have been characterized and their formation process analyzed [57,93,127]: (i) interstitial-type dislocation loops, which degenerate into dislocation tangles in time; (ii) voids; and (iii) Ga precipitates co-existing with neighboring voids. For diffusing Zn into GaAs in a Ga-rich ambient, a Zn diffused GaAs crystal

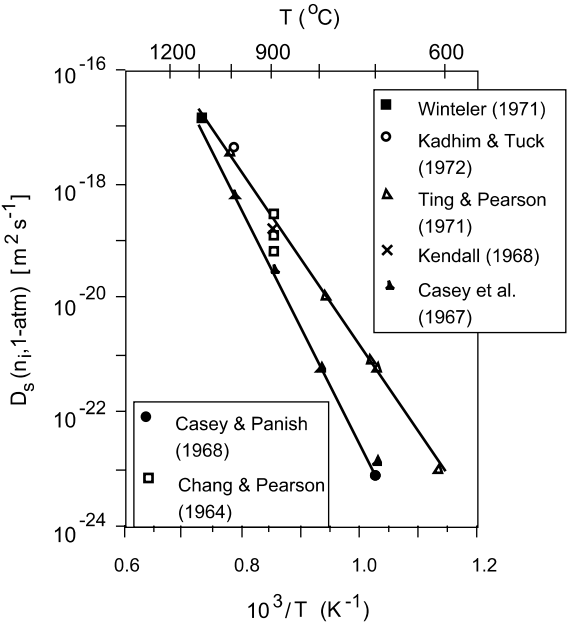

Fig. 4.20. The substitutional Zn diffusivity values under intrinsic and 1-atm As_4 pressure conditions. From [80].

region with compositions at the allowed Ga-rich boundary shown in Fig. 4.13a is obtained, irrespective of the GaAs starting composition. The fact that the Zn diffused region is indeed rich in Ga is evidenced by the presence of Ga precipitates in the voids [93]. Formation of these defects ensures the Zn in-diffusion profile to be governed by the thermal equilibrium concentrations of native point defects of the Ga-rich GaAs crystal, and the profile is box-shaped which reveals the p^2 (or C_s^2) dependence of the substitutional Zn diffusivity D_s. Such a profile is shown in Fig. 4.21 together with an illustration of the involved extended defects. It is, however, noted that the crystal is in a highly non-equilibrium state, for two reasons. First, extended defects are generated. Second, the starting material may not be rich in Ga and hence the crystal will now contain regions with different compositions which is of course a highly non-equilibrium crystal.

For diffusing Zn into GaAs in an As-rich ambient, the situation is more complicated. After a sufficient elapse of diffusion time, the crystal surface region becomes As-rich because of the presence of a high ambient As_4 pressure. But, since

$$D_i C_i^{eq} \gg D_{As}^{SD}(p) \tag{4.63}$$

holds in the Zn diffusion front region, it is Ga-rich. Thus, the high-concentration Zn in-diffusion profiles are of a kink-and-tail type resembling those of high concentration P in-diffusion profiles in Si, see Fig. 4.22. The kink-and-tail profile develops because the Zn_s solubility value in the As-rich and Ga-rich GaAs materials are different [93]. In the high Zn concentration region the

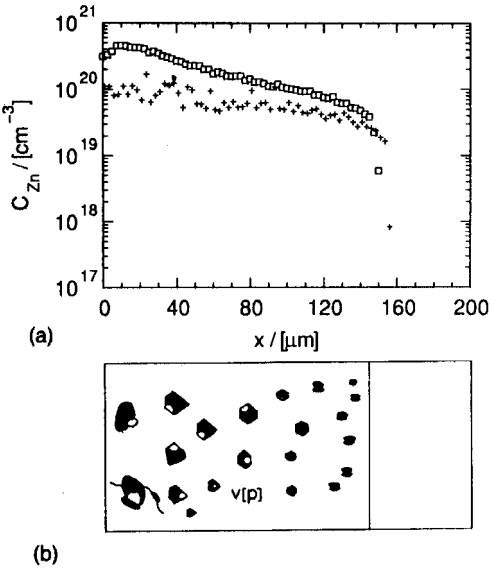

Fig. 4.21. (a) Zn in-diffusion profiles obtained at 900°C under Ga-rich ambient conditions. Squares are the total Zn concentration and crosses are the hole or Zn_s concentration. The higher total Zn concentration indicates formation of Zn containing precipitates caused by the use of a non-equilibrium Zn source material which diffused Zn into GaAs exceeding its solubility at 900°C. (b) A schematic diagram indicating the morphologies and distributions of voids (open) and Ga precipitates (filled), indicated by also v[p]. The presence of dislocations is not shown. From [93].

$D_s(n_i)$ values are those given by (4.60a) and (4.60b), while in the tail or Zn diffusion front region the $D_s(n_i)$ values are those given by (4.61a) and (4.61b). These profiles cannot be modelled with a high degree of self-consistency, because the extended defect formation process cannot be modelled without the use of some phenomenological parameters [80]. The evolution of the extended defects, as suggested by Tan et al. [57] and Luysberg et al. [127], are as follows: (i) to reduce I_{Ga}^{2+} supersaturation, they form interstitial type dislocation loops containing extra GaAs molecules, with the needed As atoms taken from the surrounding As sites which generates a V_{As} supersaturation; (ii) the supersaturated V_{As} collapses to form voids, each of an initial volume about that of a neighboring Ga precipitate formed from Ga atoms lost the neighboring As atoms to the formation of the dislocation loops. The voids will be rapidly filled by subsequently generated Ga self-interstitials due to further Zn in-diffusion. For cases of diffusing Zn into GaAs in a Ga-rich ambient, the voids contain Ga precipitates throughout the Zn in-diffused region, but for cases of diffusing Zn into GaAs in an As-rich ambient, the surface region voids are empty.

Chromium

Chromium is a deep acceptor occupying Ga sites and is used for fabricating semi-insulating GaAs. In undoped GaAs, diffusion of Cr involves no charge effects. In-diffusion profiles of Cr are characterized by a kickout type profile from the crystal surface to a substantial depth and an erfc-type profile deeper in the material near the diffusion front [60, 128]. Out-diffusion profiles are

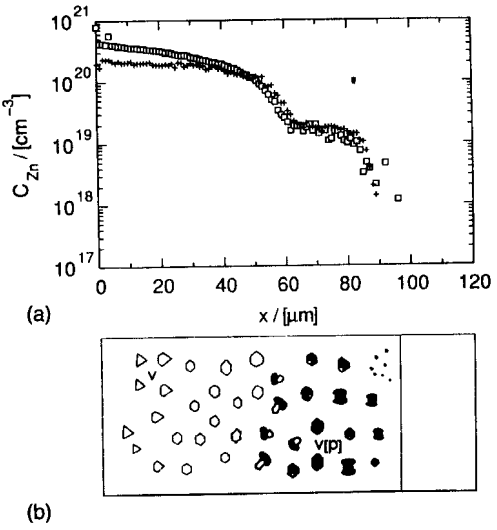

Fig. 4.22. (a) Zn in-diffusion profiles obtained at 900°C under As-rich ambient conditions. Squares are the total Zn concentration and crosses are the hole or Zn_s concentration. The higher total Zn concentration indicates formation of Zn containing precipitates caused by the use of a non-equilibrium Zn source material which diffused Zn into GaAs exceeding its solubility at 900°C. (b) A schematic diagram indicating the morphologies and distributions of voids (open) and Ga precipitates (filled). The presence of dislocations is not shown. From [93].

characterized by a constant diffusivity which is much lower than that for in-diffusion. The existence of the two types of profiles needs the description of the i-s diffusion mechanism in terms of the KO mechanism $Cr_i \Leftrightarrow C_s + I_{Ga}^{2+} + 2e$ and/or the Longini mechanism $Cr_i + V_{Ga}^{3-} \Leftrightarrow C_s + 3e$, where e denotes an electron.

Tuck [60] and Deal and Stevenson [128] have discussed Cr diffusion in terms of the Longini mechanism. The satisfactory treatment of the diffusion behavior of Cr in intrinsic GaAs [81], however, includes the co-existence of V_{Ga} and I_{Ga}, the dependence of C_s^{eq} and C_i^{eq} on the outside Cr vapor pressure, and a dynamical equilibrium between the native point defects in the Ga and the As sublattice at the crystal surface region. In-diffusion of Cr turned out to be governed by the effective diffusivity $D_{surf}^{eff} = (D_I C_I^{eq}/C_s^{eq})(C_s^{eq}/C_s)$ in the surface region, which is concentration dependent, and by the much faster constant diffusivity $D_{tail}^{eff} = D_i C_i^{eq}/C_s^{eq}$ in the tail region. The deduced $D_I C_I^{eq}$ value from Cr in-diffusion profiles [81] were included in (4.40).

In the case of out-diffusion the Cr vapor pressure is so low that, similarly to the case of out-diffusion of Zn, a much lower diffusivity prevails. This slower out-diffusion turned out to be dominated either by the constant V-dominated diffusivity $D_s^{eff} = D_V C_V^{eq}/C_s^{eq}$ or the constant S_i dominated diffusivity $D_s^{eff} = D_i C_i^{eq}/C_s^{eq}$, whichever is larger for low outside chromium vapor pressure.

Sulfur

The group VI donor S occupies As sites. With lower surface concentrations, the S in-diffusion profiles [66,129,130] resemble the erfc-function, but a concave shape develops in the surface region for higher concentration cases. The latter cases are indicative of the operation of the KO mechanism for an i-s

impurity. The available S in-diffusion profiles have been quantitatively explained [66] using the KO mechanism assuming the involvement of the neutral As self-interstitials, I^0_{As}. The deduced $D^I_{As}(n_i, 1\,\text{atm})$ values were included in (4.50).

4.5.5 Diffusion in Other III-V Compounds

Gallium arsenide is certainly the one III-V compound in which self and impurity diffusion processes have been studied most extensively. The available results on self-diffusion in III-V compounds have been summarized by Willoughby [131]. The Group III and the Group V diffusivities appear to be so close in some compounds that a common defect mechanism involving multiple native point defects appears to be the case, although no definite conclusion has been reached. There are hardly any experimental results available which would allow one to draw conclusions on the type and charge states of the native point defects involved in self-diffusion processes. Zinc is an important p-type dopant also for other III-V compounds and its diffusion behavior appears to be governed by an i-s mechanism as well. No information is available on whether the FT mechanism or the KO mechanism is operating. It can be expected that dopant diffusion induced superlattice disordering may rapidly advance the understanding of diffusion mechanisms in other III-V compounds similarly as has been accomplished in GaAs.

4.6 Conclusion

Diffusion phenomena in semiconductors are now understood to a high degree of consistency, mainly due to progresses during the last 20 years or so. In semiconductors, the lattice vacancies and self-interstitials both contribute to the crystal host atom self-diffusion and to the diffusion of substitutional impurity atoms. Often the point defects are charged which leads the diffusivity of the diffusing species to be dependent upon the crystal Fermi-level. In compound semiconductors, the diffusivity of the diffusing species will further depend on the ambient pressure of an appropriate vapor phase. The i-s diffusion mechanism appears to govern the diffusion processes of many impurities.

Notation

A_i	interstitialy dissolved atom of species A
As_{Ga}	the antisite defect of an As atom occupying a Ga-sublattice site
A_s	substitutionally dissolved atom of species A
C	carbon

C	concentration
$C_{\mathrm{x}}^{\mathrm{eq}}$ or $c_{\mathrm{x}}^{\mathrm{eq}}$	actual or normalized thermal equilibrium concentration of species x
D or D_{y}	diffusivity (diffusion coefficient) or diffusivity of species y
D^{eff}	effective diffusivity
$D_{(j)}^{\mathrm{eff}}$	effective diffusivity of a species controlled diffusion of species j
D_{s}	diffusivity of species s
D_{SD}	self-diffusion coefficient
D_{SD}^{I} or D_{SD}^{V}	I or V contribution to the self-diffusion coefficient
D_{T}	tracer self-diffusion coefficient
D_0	pre-exponential factor of D_{T} or D_{SD}
$D_{\mathrm{s}}^{\mathrm{per}}$ or $\Delta_{\mathrm{s}}^{\mathrm{per}}$	actual or normalized s diffusivity perturbed by non-equilibrium point defect concentrations
e	the electrical carrier electrons
f_I or f_V	tracer diffusion correlation factors or interstitialcy or vacancy mechanism
$\mathrm{Ga}_{\mathrm{As}}$	the antisite defect of a Ga atom occupying an As-sublattice site
h	the electrical carrier holes
h_I^{f} or h_V^{f}	formation enthalpy of I or V
h_I^{m} or h_V^{m}	migration enthalpy of I or V
i	interstitialy dissolved impurity
i-s	interstitial-substitutional impurity
I	self-interstitials
I_{Ga} or I_{As}	Ga or As self-interstitials
I_{Ga}^{2+}	doubly-positively-charged Ga self-interstitials
I^0, I^+, I^-, etc.	neutral, singly-positively-charged, singly-negatively charged I, etc.
k_{B}	Boltzmann's constant
n	donor doped or electron concentration of a semiconductor
n_{i}	intrinsic carrier concentration
p	acceptor doped or hole concentration of a semiconductor
P	pressure
Q	activation enthalpy
s	substitutionally dissolved impurity
s_I or s_V	self-interstitial or vacancy supersaturation ratio
T	absolute temperature
V	vacancies
V_{Ga} or V_{As}	Ga- or As-sublattice vacancies
V_{Ga}^{3+}	triply-negatively-charged Ga-sublattice vacancies
V^0, V^+, V^-, etc.	neutral, singly-positively-charged, singly-negatively charged V, etc.
Φ_I	interstitialcy fraction of the Si self-diffusion coefficient

References

1. A. Seeger, C.P. Chik: Phys Stat. Sol. **29**, 455 (1968)
2. T.Y. Tan, U. Gösele: Appl. Phys. A **37**, 1 (1985)
3. T.Y. Tan, U. Gösele. In: *Handbook of Semiconductor Technology, vol 1: Electronic Structure and Properties of Semiconductors*, ed by K.A. Jackson, W. Schröter (Wiley-VCH, New York 2000) pp 231–290
4. W. Frank, U. Gösele, H. Mehrer, A. Seeger. In: *Diffusion in Crystalline Solids*, ed by G.E. Murch, A. Nowick (New York: Academic Press 1984) pp 31–142
5. U. Gösele, W. Frank, A. Seeger: Appl. Phys. **23**, 361 (1980)
6. F.C. Frank, D. Turnbull: Phys. Rev. **104**, 617 (1956)
7. N.A. Stolwijk, B. Schuster, J. Hölzl, H. Mehrer, W. Frank: Physica B+C **116**, 335 (1983)
8. S. Mantovani, F. Nava, C. Nobili, G. Ottaviani: Phys. Rev. B **33**, 5536 (1986)
9. N.A. Stolwijk, M. Perret, H. Mehrer: Defect and Diffusion Forum **59**, 79 (1988)
10. M. Perret, N.A. Stolwijk, L. Cohausz: J. Phys.: Condens. Mater. **1**, 6347 (1989)
11. F.A. Huntley, A.F.W. Willoughby: Phil. Mag. **28**, 1319 (1973)
12. C. Boit, F. Lay, R. Sittig: Appl. Phys. A **50**, 197 (1990)
13. T.Y. Tan, U. Gösele: Appl. Phys. Lett. **40**, 616 (1982)
14. G.K. Celler, L.E. Trimble: Appl. Phys. Lett. **53**, 2492 (1988)
15. R. Francis, P.S. Dobson: J. Appl. Phys. **50**, 280 (1979)
16. T.Y. Tan, B.J. Ginsberg: Appl. Phys. Lett. **42**, 448 (1983)
17. S.M. Hu: Appl. Phys. Lett. **51**, 308 (1987)
18. P. Fahey, P.B. Griffin, J.D. Plummer: Rev. Mod. Phys. **61**, 289 (1989)
19. H. Strunk, U. Gösele, B.O. Kolbesen: Appl. Phys. Lett. **34**, 530 (1979)
20. C.L. Claeys, G.J. DeClerck, P.J. van Overstraeten: Rév. Phys. Appliqueé **13**, 797 (1978)
21. F.F. Morehead, R.F. Lever: Appl. Phys. Lett. **48**, 151 (1986)
22. M. Yoshida, E. Arai, H. Nakamura, Y. Terunuma: J. Appl. Phys. **45**, 1498 (1974)
23. U. Gösele. In: *Microelectronic Materials and Processes*, ed by R.A. Levy (Kluwer Academic, Dordrecht 1989) pp 588–634
24. P. Fahey, S.S. Iyer, G.J. Scilla: Appl. Phys. Lett. **54**, 843 (1989)
25. B.P.R. Marioton, U. Gösele: Jpn. J. Appl. Phys. **28**, 1274 (1989)
26. G.C. Watkins, K.L. Brower: Phys. Rev. Lett. **36**, 1329 (1976)
27. L.A. Ladd, J.P. Kalejs. In: *Oxygen, Carbon, Hydrogen and Nitrogen in Crystalline Silicon*, ed by J.C. Mikkelsen Jr, S.J. Pearton, J.W. Corbett, S.J. Pennycook (Proc. 59, Mat. Res. Soc., Pittsburgh 1986) pp 445–450
28. U. Gösele, A. Plössl, T.Y. Tan. In: *Electrochem. Soc. Proc. 96–4*, (Electcochem. Soc., Pennington 1996) pp 309–323
29. R. Scholz, U. Gösele, J.-Y. Huh, T.Y. Tan: Appl. Phys. Lett. **72**, 200 (1998)
30. R. C. Newman, J. Wakefield: J. Phys. Chem. Solids **19**, 230 (1961)
31. F. Rollert, N.A. Stolwijk, H. Mehrer: Mater. Sci. Forum **38–41**, 753 (1989)
32. R.F. Scholz, P. Werner, U. Gösele, T.Y. Tan: Appl. Phys. Lett. **74**, 392 (1999)
33. H. Rücker, B. Heinemann, W. Röpke, D. Krüger, G. Lipert, H. J. Osten: Appl. Phys. Lett. **73**, 2682 (1998)
34. P. Werner, H-J. Gossmann, D.C. Jacobson, U. Gösele: Appl. Phys. Lett. **73**, 2465 (1998)

35. P.A. Stolk, H-J. Gossmann, D.J. Eaglesham, D.C. Jacobson, C.S. Raferty, G.H. Gilmer, M. Jaraiz, J.M. Poate: J. Appl. Phys. **81**, 6031 (1997)
36. M.R. Kump, R. Dutton: IEEE Trans. CAD **7**, 191 (1988)
37. S. Mizuo, H. Higuchi: J. Electrochem. Soc. **130**, 1942 (1983)
38. D.A. Antoniadis, I. Moskowitz: J. Appl. Phys. **53**, 6788 (1982)
39. W. Taylor, B.P.R. Marioton, T.Y. Tan, U. Gösele: Rad. Eff. and Defects in Solids **111 & 112**, 131 (1989)
40. T. Sinno, R.A. Brown, W. von Ammon, E. Dornberger: J. Electrochem. Soc. **145**, 302 (1998)
41. P.S. Plekhanov, U.M. Gösele, T.Y. Tan: J. Appl. Phys. **84**, 718 (1998)
42. L. Goodwin, A.J. Skinner, D.G. Pittfor: Europhys. Lett. **9**, 701 (1989)
43. C. Nichols, C.G. Van de Walle, S.T. Pantelides: Phys. Rev. Lett. **62**, 1049 (1989)
44. C.Z. Wang, C.T. Chan, K.M. Ho: Phys. Rev. Lett. **66**, 189 (1991)
45. J. Zhu, D. de la Rubia, L.H. Yang, C. Mailhiot, G.H. Gilmer: Phys. Rev. B **54**, 4741 (1996)
46. M. Tang, L. Colombo, J. Zhu, D. de la Rubia: Phys. Rev. B **55**, 14279 (1997)
47. G. Watkins. In: *Lattice Defects in Semiconductors 1974*, ed by I.A. Huntley (Inst. Phys. Conf. Ser. 23, London 1975) pp 1–22
48. T.Y. Tan, E.E. Gardner, W.K. Tice: Appl. Phys. Lett. **30**, 175 (1977)
49. W. Kaiser, H.L. Frisch, H. Reiss: Phys. Rev. **112**, 1546 (1958)
50. R.C. Newman: J. Phys. C **18**, L967 (1985)
51. U. Gösele, T.Y. Tan: Appl. Phys. A **28**, 79 (1982)
52. A. Van Wieringen, N. Warmoltz: Physica **22**, 849 (1956)
53. S.J. Pearton, J.W. Corbett, T.S. Shi: Appl. Phys. A **43**, 153 (1987)
54. N.M. Johnson, F.A. Ponce, R.A. Street, R.J. Nemanich: Phys. Rev. B **35**, 4166 (1987)
55. N.A. Stolwijk, W. Frank, J. Hölzl, S.J. Pearton, E.E. Haller: J. Appl. Phys. **57**, 5211 (1985)
56. D.G. Deppe, N. Holonyak Jr: J. Appl. Phys. **64**, R93 (1988)
57. T.Y. Tan, U. Gösele, S. Yu: Cri. Rev. Solids Mater. Sci. **17**, 47 (1991)
58. J. R. Arthur: J. Phys. Chem. Solids **28**, 2257 (1967)
59. T.Y. Tan: Mater. Sci. Eng. **B10**, 227 (1991)
60. B. Tuck: *Atomic Diffusion in III-V Semiconductors* (Adam Hilger, Bristol 1988)
61. W.D. Laidig, N. Holonyak Jr, M.D. Camras, K. Hess, J.J. Coleman, P.D. Dapkus, J. Bardeen: Appl. Phys. Lett. **38**, 776 (1981)
62. G. Bösker, N.A. Stolwijk, H. Mahrer, U. Södervall, J.V. Thordson, T.G. Anderson, A. Buchard. In: *Diffusion Mechanisms in Crystalline Materials*, ed by Y. Mishin, G. Vogl, N. Cowern, R. Catlow, D. Farkas (Materials Research Soc., Pittsburgh 1998) pp 347–356
63. U. Egger, M. Schultz, P. Werner, O. Breitenstein, T.Y. Tan, U. Gösele U, R. Franzheld, M. Uetmatsu, H. Ito: J. Appl. Phys. **81**, 6056 (1997)
64. R. Scholz, U. Gösele U, O. Breitenstein, U. Egger, T.Y. Tan: Diffusion and Defect Data B **63–64**, 183 (1998)
65. M. Schultz, U. Egger, R. Scholz, O. Breitenstein, U. Gösele, T.Y. Tan: J. Appl. Phys. **83**, 5295 (1998)
66. M. Uematsu, P. Werner, M. Schultz, T.Y. Tan, U. Gösele: Appl. Phys. Lett. **67**, 2863 (1995)

67. H. Palfrey, M. Brown, A. Willoughby: J. Electr. Mater. **12**, 863 (1983)
68. B. Goldstein: Phys. Rev. **121**, 1305 (1961)
69. H.D. Palfrey, M. Brown, A.F.W. Willoughby: J. Electrochem. Soc. **128**, 2224 (1981)
70. L.L. Chang, A. Koma: Appl. Phys. Lett. **29**, 138 (1976)
71. P.M. Petroff: J. Vac. Sci. Technol. **14**, 973 (1977)
72. R.M. Fleming, D.B. McWhan, A.C. Gossard, W. Weigmann, R.A. Logan: J. Appl. Phys. **51**, 357 (1980)
73. J. Cibert, P.M. Petroff, D.J. Werder, S.J. Pearton, A.C. Gossard, J.H. English: Appl. Phys. Lett. **49**, 223 (1986)
74. T.E. Schlesinger, T. Kuech: Appl. Phys. Lett. **49**, 519 (1986)
75. T.Y. Tan, U. Gösele: Appl. Phys. Lett. **52**, 1240 (1988)
76. T.Y. Tan, U. Gösele: Mat. Science and Eng. **B1**, 47 (1988)
77. A. Furuya, O. Wada, A. Takamori, H. Hashimoto: Jpn. J. Appl. Phys. **26**, L926 (1987)
78. L.J. Guido, N. Holonyak Jr, K.C. Hsieh, R.W. Kalisiki, W.E. Plano, P.D. Burtham, R.L. Thornton, J.E. Epler, T.L. Paoli: J. Appl. Phys. **61**, 1372 (1987)
79. K.Y. Hsieh, Y.C. Lo, J.H. Lee, R.M. Kolbas: Inst. Phys. Ser. **96**, 393 (1988)
80. S. Yu, T.Y. Tan, U. Gösele: J. Appl. Phys. **69**, 3547 (1991)
81. S. Yu, T.Y. Tan, U. Gösele: J. Appl. Phys. **70**, 4827 (1991)
82. T.Y. Tan, S. Yu, U. Gösele: J. Appl. Phys. **70**, 4823 (1991)
83. T.Y. Tan, H.M. You, S. Yu, U. Gösele, W. Jäger, D.W. Boeringer, F. Zypman, R. Tsu, S.-T. Lee: J. Appl. Phys. **72**, 5206 (1992)
84. J.-C. Lee, T.E. Schlesinger, T.F. Kuech: J. Vac. Sci. Technol. **B5**, 1187 (1987)
85. H. Bracht, E.E. Haller, K. Eberl, M. Cardona, R. Clark-Phelps. In: *Diffusion Mechanisms in Crystalline Materials*, ed by Y. Mishin, G. Vogl, N. Cowern, R. Catlow, D. Farkas (Materials Research Society, Pittsburgh 1998) pp 335–346
86. L. Wang, L. Hsu, E.E. Haller, J.W. Erickson, A. Fischer, K. Eberl, M. Cardona: Phys. Rev. Lett. **76**, 2342 (1996)
87. P. Mei, H.W. Yoon, T. Venkatesan, S.A. Schwarz, J.B. Harbison: Appl. Phys. Lett. **50**, 1823 (1987)
88. J.A. Van Vechten: J. Appl. Phys. **53**, 7082 (1982)
89. J.A. Van Vechten: J. Vac. Sci. Technol. **B2**, 569 (1984)
90. S.R. Tatti, S. Mitra, J.P. Stark: J. Appl. Phys. **65**, 2547 (1989)
91. M. Kawabe, N. Shimizu, F. Hasegawa, Y. Nannidi: Appl. Phys. Lett. **46**, 849 (1985)
92. J. Kobayashi, M. Nakajima, T. Fukunagon, T. Takamori, K. Shida, H. Nakashima, K. Ishida: Jpn. J. Appl. Phy. **25**, L 736 (1986)
93. W. Jäger, A. Rucki, K. Urban, H.-G. Hettwer, N.A. Stolwijk, H. Mehrer, T.Y. Tan: J. Appl. Phys. **74**, 4409 (1993)
94. T.Y. Tan, U. Gösele: Mater. Chem. Phys. **44**, 45 (1995)
95. G.A. Baraff, M. Schlüter: Phys. Rev. Lett. **55**, 1327 (1985)
96. W.M. Li, R.M. Cohen, D.S. Simons, P.H. Chi: Appl. Phys. Lett. **70**, 3392 (1997)
97. Z.H. Jafri, W.P. Gillin: J. Appl. Phys. **81**, 2179 (1997)
98. P. Mei, S.A. Schwartz, T. Venkatesan, C.L. Schwartz, E. Colas: J. Appl. Phys. **65**, 2165 (1989)

99. T.Y. Tan, U. Gösele. In: *Advances in Materials, Processing and Devices in III-V Compound Semiconductors*, ed by D.K. Sadana, L. Eastman, R. Dupuis, Proc. 144 (Materials Research Society, Pittsburgh 1989) pp 221–232
100. J.W. Lee, W.D. Laidig: J. Electron. Mater. **13**, 147 (1984)
101. Y. Hirayama, Y. Susuki, H. Okamoto: Jpn. J. Appl. Phys. **24**, 1498 (1985)
102. J. Ralston, G.W. Wicks, L.F. Eastman, B.C. Deooman, C.B. Carter: J. Appl. Phys. **59**, 120 (1986)
103. N. Kamata, K. Koboyashi, K. Endo, T. Sasudi, A. Misu: Jpn. J. Appl. Phys. **26**, 1092 (1987)
104. E.P. Zucker, A. Hasimoto, T. Fukunaga, N. Watanabe: Appl. Phys. Lett. **54**, 564 (1989)
105. R.L. Longini: Solid-State Electronics **5**, 127 (1962)
106. U. Gösele, F. Morehead: J. Appl. Phys. **54**, 4617 (1981)
107. H.R. Winteler: Helvetca Physica Acta **44**, 451 (1971)
108. K. Masu, M. Konagai, V. Takahoshi: Appl. Phys. Lett. **37**, 182 (1980)
109. B. Tuck, A.J.N. Houghton: J. Phys. **D14**, 2147 (1981)
110. P. Enquis, G.W. Wicks, L.F. Eastman, C. Hitzman: J. Appl. Phys. **58**, 4130 (1985)
111. P. Enquist, J.H. Hutchby, T.J. de Lyon: J. Appl. Phys. **63**, 4485 (1988)
112. H.M. You, T.Y. Tan, U. M. Gösele, S.-T. Lee, G.E. Höfler, K.C. Hsieh, N. Holonyak Jr, J. Appl. Phys. **74**, 2450 (1993)
113. K.L. Kavanagh, C.W. Magee, J. Sheets, J.W. Mayer: J. Appl. Phys. **64**, 1845 (1988)
114. M.E. Greiner, J.F. Gibbons: J. Appl. Phys. **57**, 5181 (1985)
115. S. Yu, U. Gösele, T.Y. Tan: J. Appl. Phys. **66**, 2952 (1989)
116. C.H. Chen, U.M. Gösele, T.Y. Tan: Appl. Phys. **A69**, 313 (1999)
117. H.-M. You, U.M. Gösele, T.Y. Tan: J. Appl. Phys. **73**, 7207 (1993)
118. M. Konagai, T. Yamada, T. Akatsuka, K. Saito, E. Tokumitsu: J. Cryst. Growth **98**, 167 (1989)
119. B.T. Cunningham, L.J. Guido, J.E. Baker, J.S. Major Jr, N. Holonyak Jr, G.E. Stillman: Appl. Phys. Lett. **55**, 687 (1989)
120. T.H. Chiu, J.E. Cunningham, J.A. Ditzenberger, W.Y. Jan, S.N.G. Chu: J. Crys. Growth **111**, 274 (1991)
121. G.E. Höfler, H.J. Höfler, N. Holonyak Jr, K.C. Hsieh: J. Appl. Phys. **72**, 5318 (1992)
122. Z. Jamal, P.J. Goodhew. In: *Chemical Perspectives of Microelectronic Materials III*, ed by C.R. Abernathy, C.W. Bates Jr, D.A. Bohling, W.S. Hobson (Proc. 282, Materials Research Society, Pittsburgh 1993) p 145
123. A.J. Moll, E.E. Haller, J.W. Ager III, W. Walukiewicz: Appl. Phys. Lett. **65**, 1145 (1994)
124. C.H. Ting, G.L. Pearson: J. Appl. Phys. **42**, 2247 (1971)
125. M.A.H. Kadhim, B. Tuck: J. Mater. Sci. **7**, 68 (1972)
126. D.L. Kendall. In: *Semiconductors and Semimetals*, vol 4, ed by R.K. Willardson, A.C. Beer (Academic Press, New York 1968) pp 163–259
127. M. Luysberg, W. Jäger, K. Urban, M. Schänzer, N. Stolwijk, H. Mehrer: Mat. Sci. Eng. **B13**, 137 (1992)
128. M.D. Deal, D.A. Stevenson: J. Appl. Phys. **59**, 2398 (1986)
129. A.B.Y. Young, G.L. Pearson: J. Phys. Chem. Solids **31**, 517 (1970)
130. B. Tuck, R.G. Powell: J. Phys. **D14**, 1317 (1981)
131. A.F.W. Willoughby. In: *Defects in Semiconductors II*, ed by S. Mahajan, J.W. Corbett (North-Holland, New York 1983) pp 237–252